國立臺灣大學工學院高分子科學及工程學研究所

碩士論文

Institute of Polymer Science and Engineering

College of Engineering

National Taiwan University

Master Thesis

功能性聚對二甲苯之物理特性及鍍膜基材選擇性

Physical Properties and Selective Deposition of

Functionalized Poly-*para*-xylylenes

孫合毅

Ho-Yi Sun

指導教授: 陳賢燁 博士

戴子安 博士

Advisors: Hsien-Yeh Chen, Ph.D.

Chi-An Dai, Ph.D.

中華民國 105 年 7 月

July, 2016

致謝

　　碩士的時間過的很快，也讓我成長了很多。對於一個碩士生來說，這兩年我過的相當豐富精采，修了不同有趣的課，完成了了許多期刊論文及專利，參加各式國內外的研討會。在這樣的過程當中，除了吸收專業的實務經驗，也學習了如何從問題，找出解決的辦法，最後一步一步的達到目標。

　　能夠順利的完成碩士的研究，一路上受到了很多人的幫助。首先感謝指導教授陳賢燁老師和戴子安老師在我研究所期間的指導與討論。特別是陳賢燁老師，給予我研究上很自由的發揮空間，讓我的想像力及創意可以實際的運用在不同的研究當中。此外，也鼓勵我多多參加不同的研討會，投稿國際期刊，讓這些研究成果得以被更多人所看到。在最後碩士論文口試的時候，除了指導教授以外，也很感謝口試委員游佳欣老師和趙玲老師。百忙之中抽空出席，指出研究中需要改進的地方，也從不同的角度為這些研究帶來新的靈感。

　　在研究室的日常生活，最感謝從我大學三年級到碩士二年級時時，生物介面工程實驗室裡的所有成員。包括了曾經指導過我的學長姊們：治宇博士、孟諭、庭如、巧慈、張鎮、勇智、姝昀、信穎、逸潔、嬿晴，與我一同在實驗室的同學們：振禹、睿宏、成遠、鼎弼。這是一個相當歡樂的研究環境，除了實驗上的切磋琢磨，踏出實驗室大家更是互相成長的夥伴，在這幾年的時光品嚐各種喜怒哀樂。

　　最後，要感謝在研究生活之外支持我的家人以及女朋友，提供了經濟與精神上的支持。除了對於我目標的肯定，還要包容我每天早出晚歸，沒辦法時時刻刻保持聯絡，而在我徬徨的時候，給予我方向與鼓勵。

　　碩士的生活真的告一段落了，成就了一個更加充實的自己。希望帶著這些經驗以及大家的祝福，往人生的下一個目標前進。

I

摘要

　　藉由化學氣相層積技術所製備之聚對二甲苯高分子鍍膜，提供了良好的表面特性，創造了生物相容性，也提供選擇性改質的應用。這樣子的鍍膜技術，除了有強韌的附著性之外，更可以應用於各種不同的物質材料以及生醫裝置上。我們也透過相關的生物測試，證實此鍍膜技術在生醫領域上的應用。最後，透過表面能量的改變，讓聚對二甲苯高分子鍍膜具備選擇性表面改質的特性。

　　在這篇研究中，一開始我們使用了功能性聚對二甲苯高分子作為作為鍍膜，設計具有各種生醫功能的材料。研究的材料除了平面的基材外，也使用了立體結構的骨釘、骨板。這些材料進行了熱穩定測試以及機械強度測試，來證明以聚對二甲苯高分子作為生醫材料鍍膜的穩定特性。更進一步的，透過在鍍膜表面修飾蛋白質分子，給予這些材料良好的生物相容性。這些具有不同尾端的蛋白質分子，在表面造成了不同的特性，可以用來控制蛋白質貼附及細胞的吸附。透過上述的鍍膜技術應用於生醫材料，除了擁有強韌的物理特性及穩定性，更是一個很好的界面，在生物環境中控制不同的生物反應。

　　在了解優異的表面物理特性後，進一步的，我們透過由下而上 (bottom-up) 的表面圖樣 (patterning) 技術，發揮聚對二甲苯高分子在表面改質精準度上的的優點。然而在過去，這樣的技術受限於基材的選擇。在這篇研究的第二部分，我們研究了一個可以被廣泛運用的技術，讓聚對二甲苯高分子可以選擇性的層積在表面上。在進行化學氣相層積的過程中，透過電場在基材的表面提供高能量，成功的抑制聚對二甲苯高分子在特定位置的層積。這樣子的技術，克服了過去在基材以及官能基上的限制，為聚對二甲苯高分子在由下而上選擇性表面改質上，提供了更廣泛的應用。

關鍵字：化學氣相層積、聚對二甲苯、鍍膜穩定性、導電表面、選擇性化學氣相層積、表面圖樣、表面改質

Abstract

Poly-*para*-xylylene coatings prepared by chemical vapor deposition can tailor surface properties through specific conjugation reactions, create effective biological functions, and provide selective surface modification. The coating technology gives a robust adherent property to a variety of substrate materials, allowing for facile and versatile application, as well as contributing a precise selective surface modification in next-generation implantable devices, cellular assays, tissue engineering, and regenerative medicine applications.

In this present study, we have used functionalized poly-*para*-xylylene polymers as coatings for the design of biological functions on various substrates. A thermal stability test against elevated temperature was used to test these coatings on selected substrates, and mechanical stability against harsh scratch test was also tested on flat substrates as well as on a bone plate/screw device. Furthermore, biofunctional activities are performed via immobilization of PEG and functional peptides based on specific conjugation using functional sites of the coatings. Tailored surface functions are created using these coatings as a result of their antifouling properties and ability to control cell attachment. The coatings reported herein provide (i) robust coating stability on a wide range of substrate materials that are commonly used in biomedical applications and (ii) designable

interfaces to mimic biological environments for controlled biological responses.

After the important interface material of poly-*para*-xylylenes has been demonstrated to be a robust tool to modify material surfaces to impart precise surface properties, with the bottom-up patterning approach, poly-*para*-xylylenes coatings provides intrinsic advantages associated with unlimited resolution but is limited by the materials available for selection. A general and simple approach towards the selective deposition of poly-*para*-xylylenes is introduced in this research. The chemical vapour deposition (CVD) of poly-*para*-xylylenes is inhibited on the high-energy surfaces of electrically charged conducting substrates. This technology provides an approach to selectively deposit poly-*para*-xylylenes irrespective of the substituted functionality and to pattern these polymer thin films from the bottom up.

Content

VIII

List of Tables

List of Figures

Chapter 1 Introduction

1.1 Biomedical Material Application

The development of biomaterials and biomedical devices has recently focused on the design of biomimetic functions that are capable of creating biological inertness to repel non-specific fouling substances, including small molecules, proteins, cells and microorganism.[1] On the other hand, biomaterials with surface functions are also being developed to elicit specific cellular responses or to direct tissue-mediated biomolecular recognition.[2] For example, biomaterials have been achieved by surface and bulk modification by attaching poly(ethylene glycol) (PEG) to suppress fouling properties,[3] or attract extracellular matrix (ECM) proteins.[4, 5] As well as short peptide sequences,[6] which can induce specific interactions with cell receptors. Percutaneous or indwelling implants are being installed with antibiotic/antiseptic ingredients for inhibition of bacterial colonization, which is the cause to peri-implantitis or peri-implantoclasia.[7, 8] Drug-eluting coatings are applied on stent devices to decrease the reoccurrence rate of blockage (restenosis) compared to bare metal stents,[9] among many more applications. In most cases, a durable and efficient performance of a surface modification method depends critically on the adhesion between the surface coating and the substrate materials. Many reports have shown that the long-term success of medical implants is impeded by

1

an unacceptable rate of deformation, such as slip bands, surface twins, surface cracks,

orange peel phenomena or ridging and roping of the coatings.[10] These topographic and

structural changes are susceptible to influence the adhesion and cohesion properties of

the coating, leading to coating failures and potentially resulting in a high risk of toxicity

to the surrounding tissue.[11]
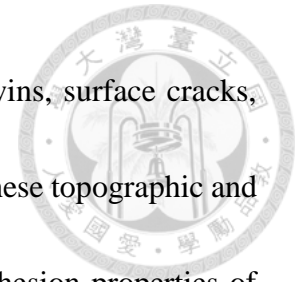
1.2 Surface Modification Approach

The emerging concept of imparting chemical or biological functionalities to material surfaces has shown promise.[4, 12, 13] A delicate presentation of these functions in the regions of interest on material surfaces can be achieved by

    a. Surface patterning

    b. Surface compositional gradients

    c. Multifunctional presentations of a and b.

These modifications with spatial definition and precision demonstrate determinantal impacts on cytoskeletal organization, proliferation, cell differentiation, gene expression, and apoptosis.[14-16] Patterning approaches are collectively discussed by top-down techniques,[17] which, although they are widely exploited due to their well-established process and availability, are limited by the resolution and dimensional characteristics of the substrates.[18] The approach by bottom-up techniques, in contrast, offer precise resolution but require substantial knowledge of how to perform the modification processes and are usually applied in solution-based methods that are applicable only for selected materials.[19, 20]

3

1.3 Functionalized Poly-*para*-xylylenes

Functionalized Poly-*para*-xylylenes(PPXs) constitute a versatile class of reactive polymers that can be used for the design of biological functions for biomaterials. These polymers can be synthesized similarly to their commercial siblings, namely, parylene,[21, 22] by using vapor-phase pyrolysis of paracyclophanes to provide conformal and pinhole-free coatings.[23] In addition, the functionalized version of these polymers exhibit excellent biological properties, as was shown by our group[24] and others,[25, 26] allowing for precisely immobilized biomolecules,[27, 28] well-controlled protein adsorption,[29, 30] and manipulated cell growth.[31, 32] More recently, the developments of these functionalized coatings have advanced to a multifunctional repertoire toward a more sophisticated mimicry of biointerface design.[33-35] The robust property of these functionalized PPXs in deed have been well-demonstrated and have shown promising successes, however their adhesion property has not yet been studied in detail.
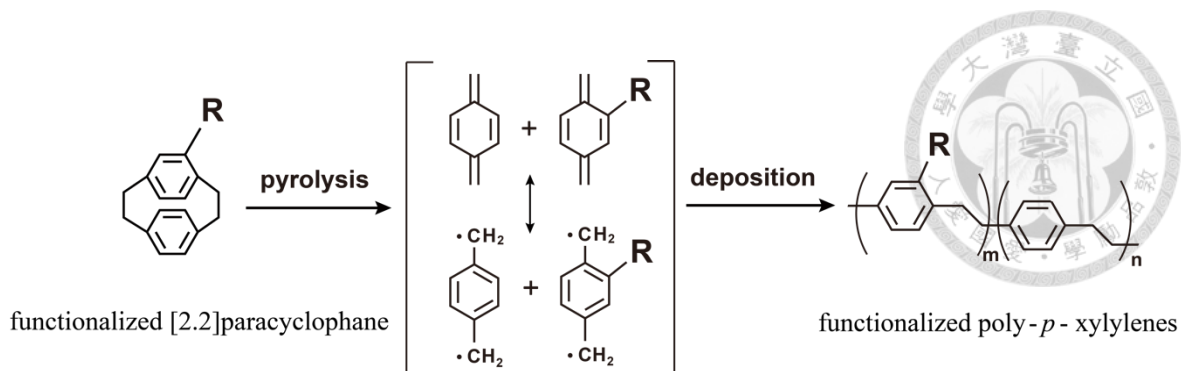
Figure 1-1 Illustration of polymerization PPXs via CVD.
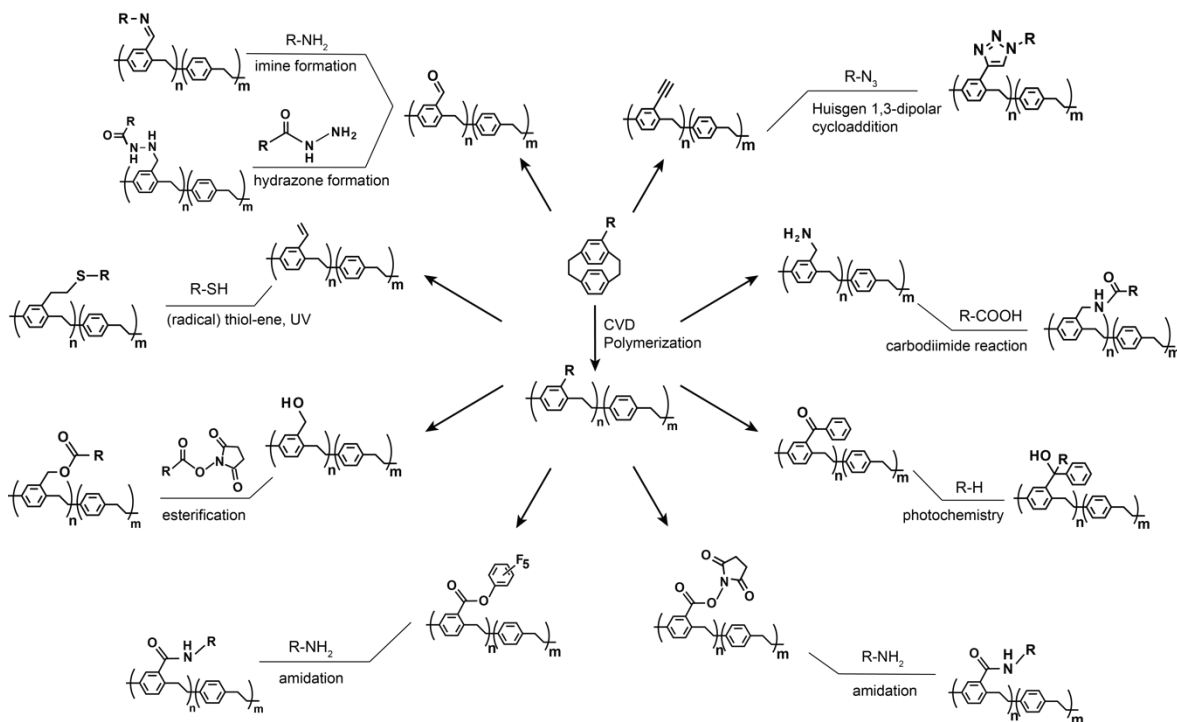
Figure 1-2 Illustration of diversified functionalities of PPXs.

1.4 Research Motivation and Specific Aims

In this study, we have used PPX polymers as coatings for the design of biological functions on various substrates, including titanium alloy (Ti6Al4V), stainless steel (SS), polymethyl methacrylate (PMMA), polystyrene (PS), polycarbonate (PC), silicon, glass, and ceramic. A thermal stability test against elevated temperature was used to test these coatings on selected substrates, and mechanical stability against harsh scratch test was also tested on flat substrates as well as on a bone plate/screw device. Furthermore, biofunctional activities are performed via immobilization of PEG and functional peptides based on specific conjugation using a thiol-ene click reaction and a thiol-maleimide coupling reaction, respectively, on vinyl and maleimide functional sites of the coatings. Tailored surface functions are created using these coatings as a result of their antifouling properties and ability to control cell attachment. The thiol-reactive coatings reported herein provide

a. Robust coating stability on a wide range of substrate materials that are commonly used in biomedical applications

b. Designable interfaces through immobilizing tailored thiol-molecules to mimic biological environments for controlled biological responses.

6

After the important interface material of PPXs has been demonstrated to be a robust

tool to modify material surfaces to impart precise surface properties, applications using

PPX coatings are commonly seen in electronic circuits, bioelectronics, conducting

electrodes, and sensors.[36, 37] The modification of using PPXs to enable top-down

modifications of selected regions has been achieved by microcontact printing (μCP),[38,

39] vapour-assisted patterning (VAMPIR),[40] and mask-assisted[41, 42] or maskless

photopatterning.[43, 44] Bottom-up demonstration using PPXs relies on the material-

dependent selectivity during the vapour deposition process and has been reported by using

transition metal substrates for non-functionalized PPXs[45-47] and vinyl-functionalized

PPX.[48] Patterning poly-*para*-xylylenes using the selective deposition of the bottom-up

approach offers advantages in not only the feature resolution but also the simpler and

more straightforward formation of the patterned layer compared with the top-down

approach. A homogeneous layer of PPX will need to be applied to the material surface

prior to performance of the patterning procedure. However, the quest for a general method

to perform the selected deposition of PPXs remains unresolved. A more general concept

of selective deposition of nonfunctional PPXs will provide a protective coating in the

region when protection is needed, and functionalized PPXs additionally enable the

immobilization of specific biomolecules and render a functional material interface in the

same regional manner.

7

Chapter 2 Materials and Methods

2.1 Experimental Instrument and Consumable Materials

2.1.1 Experimental Instrument

a. Infrared reflection absorption spectroscopy (IRRAS): Perkin Elmer Spectrum 100 FT-IR spectrometer

b. Scanning electron microscope (SEM): FEI, Nova^{TM} NanoSEM 230

c. Quartz crystal microbalance (QCM): ANT Technologies Co., Taiwan

d. Fluorescence microscopy: TE-2000U, Nikon, Japan

2.1.2 Consumable Materials

The following materials were obtained commercially and used as received, unless otherwise noted: titanium alloy (Ti6Al4V, Structure Probe Inc., USA), silicon wafer (Goldeninent Inc., Taiwan), polymethyl methacrylate (PMMA, Taifonacrylic Co., Taiwan), polystyrene (PS, Taifonacrylic Co., Taiwan), polycarbonate (PC, Sin-Shun Enterprise Co., Taiwan), stainless steel (SS, Structure Probe Inc., USA), glass (FEA, Germany), ceramic (MeiTek Inc., Taiwan), and cysteine-containing peptide, Cys-Arg-Glu-Asp-Val (CREDV) (Yao-Hong Biotechnology Inc., Taiwan). Gold substrates were fabricated from a 4 in. silicon wafer with a titanium layer of 300 Å followed by deposition

8

of a gold layer of 725 Å using a thermal evaporator (Kao Duen Technology Co., Taiwan).

An upper extremity shaft locking plate system (A-Plus Biotechnology Co., Taiwan) was

cleaned using ethanol before conducting the coating process by CVD.

Conducting glasses with fluorine-doped SnO_2 (FTO; NSG America Inc., USA) were

commercially obtained and cleaned with deionized water and isopropyl alcohol before

use. Metal substrates were fabricated from a 4-inch silicon wafer with a 3500-Å insulating

layer of silicon nitride followed by a 1000-Å metal layer. The metals of Ti, Cu, Ag, Au,

and Zn were prepared using a thermal evaporator (Kao Duen Technology Co., Taiwan).

All metal pellets were purchased from Goldeninent Inc. (Taiwan). The patterned Al

samples were fabricated with a thermal evaporator (Kao Duen Technology Co., Taiwan)

on glass substrates. Photomasks with selected corresponding patterns were designed

using AutoCAD and were printed on a high-resolution emulsion transparency (TKK,

Taiwan) with a spatial resolution of 10,000 dpi. Photomasks were used during the

photolithography process to generate the Al patterns.

2.2 Synthesis of poly-*para*-xylylenes

2.2.1 CVD Polymerizations

The synthesis of PPXs using a CVD polymerization process was conducted following a previously reported procedure.[31, 32] PPXs were deposited on substrates using CVD polymerization from their monomers mentioned above respectively. During the CVD polymerization process, the starting material was sublimed under vacuum at 100 - 110 °C and transformed into reactive species by pyrolysis from 670 - 780 °C respectively. Following pyrolysis, the resulting quinodimethanes (diradical monomers) were transferred to the deposition chamber, where polymerization occurred on a rotating holder maintained at 15 - 23 °C to ensure the uniform deposition of the polymer and the wall temperature was adjusted to 90 °C to prevent any residual deposition on the chamber walls. A pressure of 120 mTorr was maintained during the entire CVD polymerization process.

Depending on the specific study of interest, deposition rates were controlled at 0.3 Å/s - 20 Å/s, as monitored by an in situ QCM system. Electrically charged substrates were prepared by providing DC currents to the substrates using a GPS 3030D power supply (Good Will Instrument, Taiwan). Silver wires were used for the connection between the substrate and the power supply, and an electroconductive paste Dotite XA-3499 (Fujikura Kasei, Japan) was used to secure the connection joints.

10

Table 2-1 Parameters of Functionalized PPXs Polymerization

Functionalized PPXs	PPX-alkene	PPX-maleimide	PPX-C	PPX-aldehyde	PPX-TFA	PPX-amine
Pyrolysis Temperature (°C)	670	780	670	680	670	670
System Pressure (mTorr)	120	120	120	120	120	120
Holder Temperature (°C)	15	15	15	15	15	23
Carrying Gas Flow Rate(sccm)	20	50	25	20	30	20
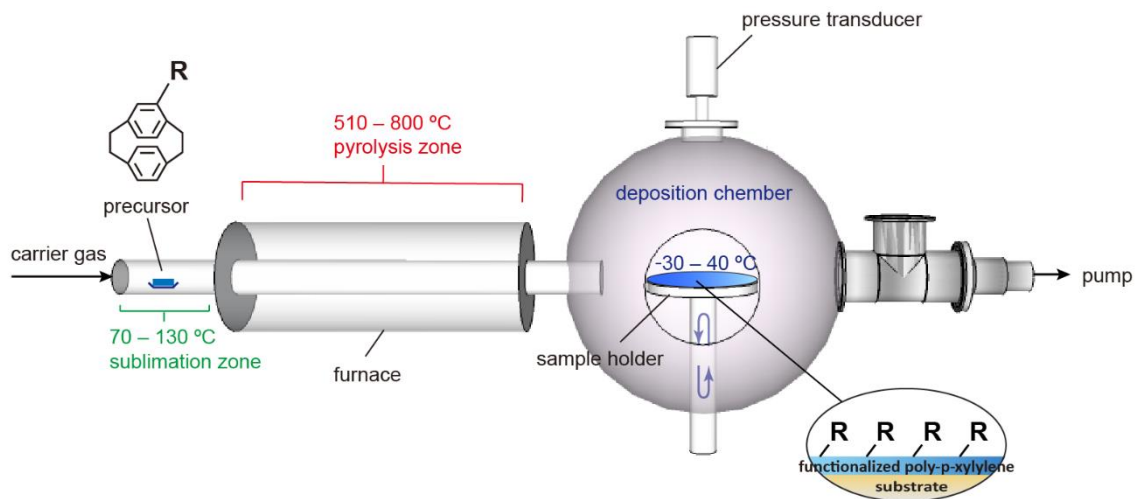
Figure 2-1 Illustration of CVD polymerixzation.

11

2.2.2 Poly(4-vinyl-*p*-xylylene-*co*-*p*-xylylene): PPX-alkene
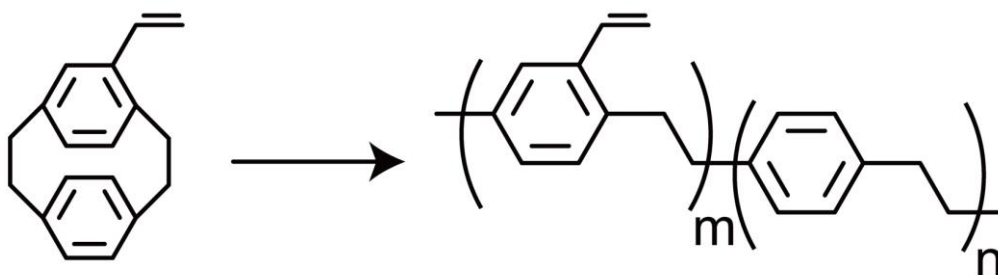
Figure 2-2 Synthesis of PPX-alkene.

2.2.3 Poly(4-N-maleimi-domethyl-*p*-xylylene)-*co*-(*p*-xylylene): PPX-maleimide
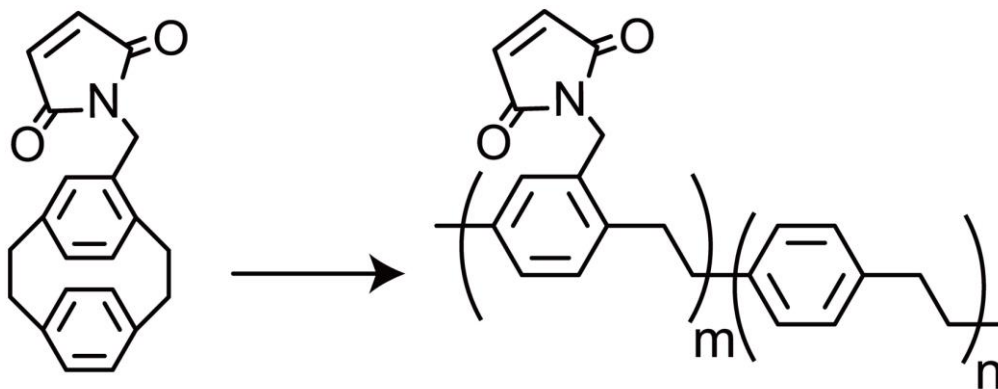
Figure 2-3 Synthesis of PPX-maleimide.

12

2.2.4 Poly(dichloro-*p*-xylylene)-*co*-(*p*-xylylene): PPX-C
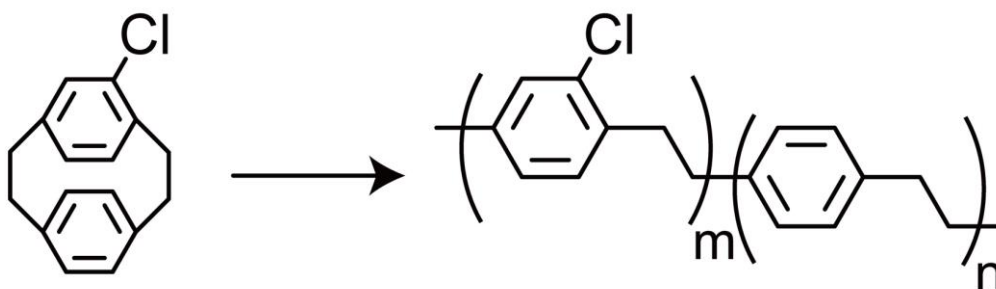
Figure 2-4 Synthesis of PPX-C.

2.2.5 Poly(4-formyl-*p*-xylylene)-co-(*p*-xylylene): PPX-aldehyde
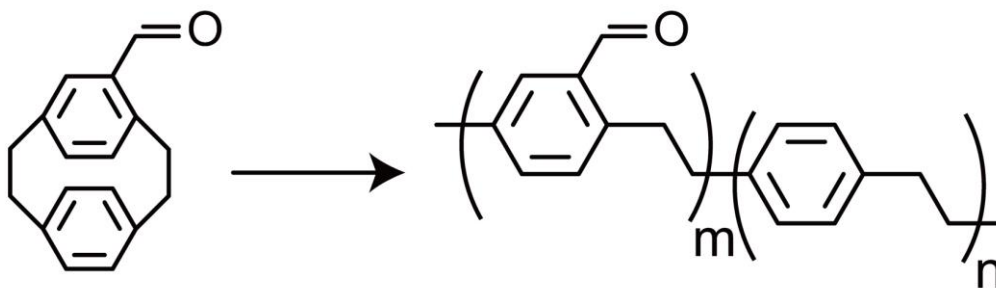
Figure 2-5 Synthesis of PPX-aldehyde.

2.2.6 Poly(4-trifluoroacetyl-*p*-xylylene)-co-(*p*-xylylene): PPX-TFA
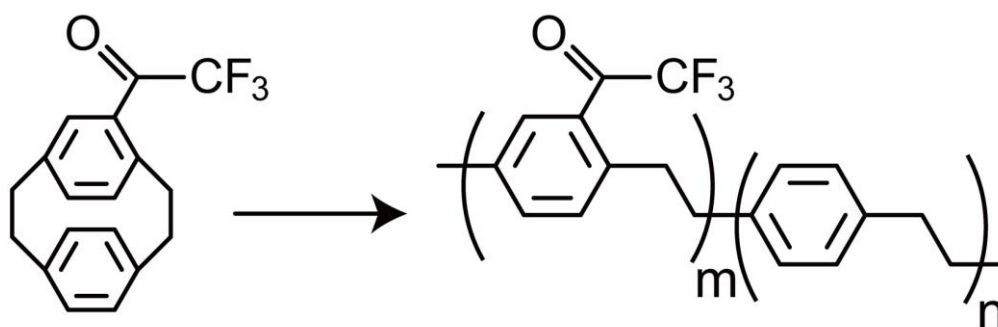
Figure 2-6 Synthesis of PPX-TFA.

2.2.7 Poly(4-aminomethyl-*p*-xylylene)-co-(*p*-xylylene): PPX-amine
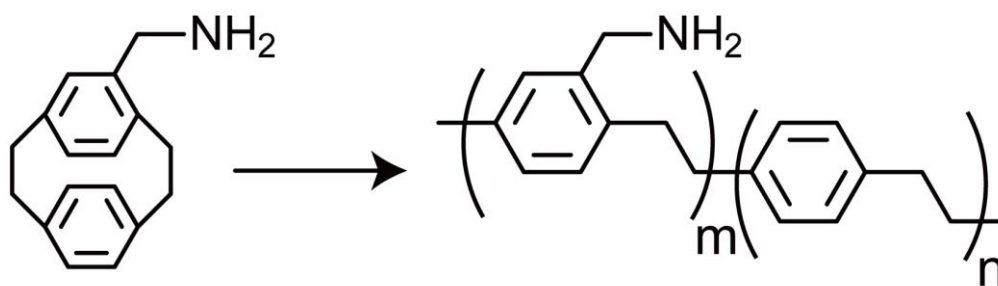
Figure 2-7 Synthesis of PPX-amine.

2.3 Surface Characterizations

2.3.1 Infrared reflection absorption spectroscopy Characterizations

The chemical compositions of the coatings were characterized using IRRAS equipped with a liquid nitrogen cooled MCT detector and a grazing angle specular reflectance accessory (AGA, Pike Technologies). The CVD coatings were attached on gold-coated silicon substrates (Au/Si) for the measurements with a blank substrate as reference.

2.3.2 Scanning Electron Microscope

A SEM that was operated at a primary energy of 5 keV and a pressure of 5×10^{-6} Torr in the specimen chamber. The samples were prepared by drying the nanoparticle solutions onto a piece of silicon wafer in drying oven at 70 °C and coating them with a conductive platinum layer before the SEM analysis.

2.3.3 Energy Dispersive X-ray Spectroscopy

The elemental analysis was confirmed by energy dispersive X-ray spectroscopy (EDS), which was performed on a SEM. The EDS was operated at a primary energy of 5 keV with a pressure of 5×10^{-6} Torr in the specimen chamber. The film thickness analysis was recorded using a stylus-based surface profiler (Dektak 6M, Veeco, USA).

2.3.4 Cross-cut Tape Adhesion Test

Adhesion strength of the coatings were analyzed by using a multi-blade cross-cut tester (ZCC 2087 cross-cut tester, Zehntner) on substrates that were coated with PPX-maleimide. In detail, the cross-cut tester was utilized to create two sets of crosswise scratches on coated substrates. Subsequently, a piece of Scotch tape was applied and removed steadily from the scratched samples within 0.5 to 1.0 second with a pulling direction angle of 60 degrees. The resulting samples were imaged with a digital camera (Nikon, D80 with lens 18–200 mm), and the test results were evaluated following the cross-cut scale of ASTM D3359.[49]

2.3.5 Bone Plate/Screw Device Adhesion Test

Adhesion strength of the coatings was tested on a PPX-alkene-deposited bone plate/screw device; a locking process was then performed to lock the screw tightly on the bone plate using a torque screw driver (A-Plus Biotechnology Co., Taiwan), followed by an unlocking process to loosen the screw from the plate using the same screw driver. The resulting plate and screw surfaces were examined using SEM. The stability of the chemical compositions of the coatings and the attached molecules were verified by using IRRAS. Spectra were recorded and compared before and after the cross-cut tape adhesion test.

16

2.4 Surface Modifications

2.4.1 Bioconjugation Reactions

Cysteine-containing peptide, CREDV and thiol-terminated poly(ethylene glycol)

PEG were immobilized on PPX-alkene and PPX-maleimide via a thiol-maleimide

coupling reaction or a thiol-ene click reaction. For the thiol-maleimide coupling reaction,

CREDV (4 mg mL^{-1}) or PEG (100 mg/mL) solutions were applied on the surfaces of

PPX-alkene at room temperature (25 °C) for 2 hours. The resulting samples were then

washed with phosphate-buffered saline (PBS, pH = 7.4; contains Tween 20, Sigma) three

times and twice with PBS (pH = 7.4, Sigma), rinsed with deionized water, and finally

dried using a stream of compressed nitrogen gas. For the thiol-ene reaction, CREDV (4

mg mL^{-1}) or PEG (100 mg/mL) solutions were applied on the surfaces of PPX-maleimide

in the presence of photoinitiator of *2,2-dimethoxy- 2-phenylacetophenone* (50 mM, Sigma

Aldrich) and a UV irradiation using 365 nm wavelength was conducted for 5 minutes

(OmniCure, S1500) to initiate the reaction. The resulting samples were also flushed by

PBS-tween buffer solution 3 times, PBS twice, deionized water once, and finally dried

with a stream of compressed nitrogen gas.

2.4.2 Quartz Crystal Microbalance Analysis

A QCM was equipped with a flow injection analysis (FIA) device and continuous frequency-variation recording device. The sensing element of this instrument was an AT-cut piezoelectric quartz disk with a resonant frequency of 9 MHz, and a total sensing area of 0.1 cm^2 through coating alkene-PPX or maleimide-PPX and reacted PEG-thiol, respectively, by thiol-ene reaction or thiol- maleimide reaction for monitoring in situ the response of protein adsorption. The FIA device was turned on and a flow rate of 36.5 μl min−1 was maintained using a peristaltic pump. The carrier solution (PBS, pH = 7.4) was continuously delivered into the flow channel until a stable frequency response was obtained. BSA was then dissolved in a solution of the same composition as the carrier solution, at a BSA concentration of 312.5 μg mL^{-1}. An aliquot of 100 μl of BSA was injected into the flow system. The time-dependent change in frequency was recorded continuously using a frequency meter, and the data were stored in a computer throughout the detection of the protein adsorption.

18

2.4.3 Cell Culture and MTT Assays

PPX-alkene and PPX-maleimide were deposited on stainless steel (SS) substrates, and the coated substrates were then modified with different conditions following previously described orthogonal conjugations to obtain six types of samples: PEG-immobilized PPX-alkene, PEG-immobilized PPX-maleimide, bare SS surface, as-deposited Coating PPX-alkene, as-deposited PPX-maleimide, CREDV-immobilized PPX-alkene, and CREDV- immobilized PPX-maleimide. The samples were then used for culture of human umbilical vein endothelial cells (HUVECs). (HUVECs) were obtained commercially from ScienCell Research Laboratories (catalog #8000) and were cultured on the six types of samples in M199 (Sigma-Aldrich Co., USA) containing 10% fetal bovine serum (FBS) for 24 hours at 37 °C in a humidified, 5% $CO_2 - 95\%$ air atmosphere. For the cell viability assay, 3-[4,5-dimethylthiazol-2-yl]-2,5-diphenyl tetrazolium bromide (MTT) solution (Sigma-Aldrich Co., USA) was added to each well and incubated for 3 hours at 37 °C. After incubation, MTT was aspirated, and dimethyl sulphoxide (DMSO) was added. Subsequently, the MTT solution was aspirated, and the formazan crystals that formed were dissolved in DMSO. The spectrophotometric analysis was run at 570 nm using a multi-well plate reader. (PowerWave X; Bio-Tek, Winooski, VT, USA)

2.4.4 Immobilization

The immobilization of the Alexa Fluor® 568-conjugated hydrazide (Thermo Fisher Scientific Inc., USA) was conducted using a 5 mM concentration on the patterned PPX-aldehyde samples for 1 hr. A washing procedure was performed after the reaction using phosphate-buffered saline (PBS, pH = 7.4; containing Tween 20, Sigma-Aldrich, USA) three times and PBS (pH=7.4, Sigma-Aldrich, USA) one time and, finally, rinsing with deionized water. The resulting samples were then examined by fluorescence microscopy.

2.5 Sticking Coefficient

The calculation of the value of *S* for the deposition of PPXs was performed following the reported model and equations.[23] This model is based on the fact that the maximum deposition rate (R_d) for any CVD process can be given by:

$$R_d = \frac{SPN_aV_m(6\times10^{11})}{(2\pi m_rRT_0)^{0.5}}$$
(Eq 1)

where the quantity $\frac{PN_aV_m(6\times10^{11})}{(2\pi m_rRT_0)^{0.5}}$ is the flux of the reactant to the substrate surface in collisions per square metre per second, *P* is the pressure in pascals, N_a is Avogadro's number, m_r is the molecular mass in kilograms per mole, *R* is the Rydberg gas constant, T_0 is the temperature of the reactant gas in kelvin, and V_m is the volume of one molecule in cubic meters.

Thus, the expression for *S* is

$$S = \frac{R_d\times(2\pi m_rRT_0)^{0.5}}{PN_aV_m(6\times10^{11})}$$
(Eq 2)

The value of *S* was calculated for PPX-C on three surfaces that represented three different cases:

21

a. A silicon (Si) surface represented an uncharged, non-inhibitory surface

b. An iron (Fe) surface was used as an inhibitory surface (it was previously reported to be the best inhibitor)

c. A charged aluminium (Al) surface with an applied charge density of 0.05 C/cm^2 was used to represent charged inhibition.

Deposition parameters including temperature = 300 K, system pressure = 15 Pa and deposition rate = 2000 Å/min for Si, 300 Å/min for Fe and 30 Å/min for charged Al were used for the calculation to obtain values of $S = 1.29 \times 10^{-4}$ for Si, $S = 1.94 \times 10^{-5}$ for Fe and $S = 1.94 \times 10^{-6}$ for charged Al.
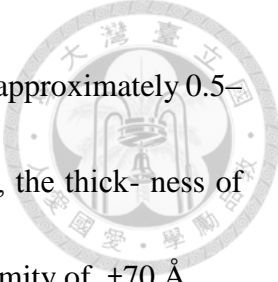
Chapter 3 Physical Properties

3.1 Coating Stability

3.1.1 CVD Polymerization
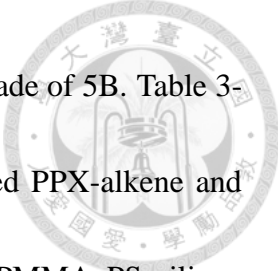
PPX-alkene and PPX-maleimide were synthesized from their corresponding starting

materials of 4-vinyl-[2.2]paracyclophane and maleimidomethyl-[2,2]paracyclophane,

respectively, via a refined chemical vapor deposition (CVD) polymerization process

following previously reported conditions.[32, 48, 50] During the CVD process, a

sublimation temperature of 100–110 °C was used to sublime 4-vinyl-[2.2]paracyclophane

or maleimidomethyl-[2,2]paracyclophane; and the sublimed paracyclophanes were

transferred to the pyrolysis zone that exposed the compounds to temperatures of 580 °C

or 670 °C, and the *C-C* bonds of the paracyclophanes were cleaved to generate the

corresponding *p*-quinodimethanes (monomers).[51] During the last step, the monomers

copolymerized upon condensation on a cooled substrate, forming PPX-alkene and PPX-

maleimide on the substrate. Substrate materials that are commonly used for biomedical

application, such as titanium alloy (Ti6Al4V), stainless steel (SS), polymethyl

methacrylate (PMMA), polystyrene (PS), polycarbonate (PC), silicon, glass, and ceramic,

were selected for the CVD of PPX-alkene and PPX-maleimide in the study. A quartz

crystal microbalance (QCM) was used to confirm the coating thickness after retrieving

23

the samples from the deposition chamber. A controlled growth rate of approximately 0.5–

1 Å s−1 was maintained to ensure the coating quality. Consequently, the thick- ness of

the coating on the substrates was approximately 2000 Å with a uniformity of ±70 Å.

3.1.2 Adhesion Property

Mechanical stability of the coatings against different substrate materials were tested

based on a cross-cut tape adhesion test. A multi-blade cross-cut tester was utilized to

create two sets of cross- wise scratches on the coated substrate, and a piece of Scotch tape

was then applied and removed steadily from the scratched samples within 0.5 to 1.0

second using an angle of 60 degrees for the pulling direction. The tested coatings were

examined using a digital camera to obtain images of the sample before and after the tape

was removed. Figure 3-1, (a) and (b) are showing the test performed on a silicon substrate

which is coated by PPX-alkene. The images were recorded before and after the tape was

removed from the coating surface. (c) and (d) are showing the test performed on a

Ti6Al4V substrate which is coated by PPX-maleimide, and the images were recorded

before and after the tape was removed from the coating surface. This comparison for

samples with PPX-maleimide-deposited on silicon and Ti6Al4V, and no discernable

damage or delamination was found at the cut edges or on the area of the remaining coating.

The results were also evaluated following the cross-cut scale of ASTM D3359[49] that

24
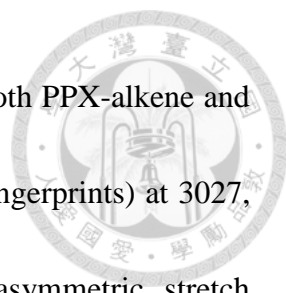
classifies a worst film adhesion strength of 0B grade and a highest grade of 5B. Table 3-1 summarizes the cross-cut tape adhesion test results of as-deposited PPX-alkene and PPX-maleimide on different substrates, namely Ti6Al4V, Au, SS, PC, PMMA, PS, silicon, glass, and ceramic, and the highest 5B level was found for both PPX-alkene and PPX-maleimide on all the substrates tested. The results reveal that ultrathin PPX-alkene and PPX-maleimide (with a thickness of approximately 2000 Å) can exhibit excellent adherence and cohesive properties on these substrates, which is evidently sup- ported by the fact that an increased film thickness is prone to increase the interfacial shear stress between the coated film and the underlying substrate, following the equation below:

$$d \cdot \sigma_{yy} = \int \tau(y) dy \qquad \text{(Eq 3)}$$

where d is the thickness of the film, $\tau(y)$ is the interfacial shear stress and σyy is the film stress.[52]

3.1.3 IRRAS Characterizations

Coating stability with respect to the change of chemical structure was further examined by using infrared reflection absorption spectroscopy (IRRAS) analysis, which is advantageous to acquire quantitative comparison for identical samples.[53, 54] The

25

spectra were compared before and after the cross-cut tape test for both PPX-alkene and

PPX-maleimide. As indicated in Figure 3-2, characteristic bands (fingerprints) at 3027,

2927, and 2858 cm^{-1} were recorded for the symmetric and asymmetric stretch

corresponding to –C–H absorptions, and peaks at around 1674 cm^{-1} attributed to the

unsaturated –C = C– stretch, were also detected for PPX-alkene before the tape-removing

step of the cross-cut tape test. After completing the test to remove the tape from the

scratched surfaces, these fingerprint peaks were found intact with no change in peak

position or intensity. Similarly, characteristic peaks at 1767 and 1706 cm^{-1}, attributed to

the asymmetric stretching of –C = O, and a peak at 1396 cm^{-1}, attributed to the symmetric

stretch of C–N–C from the maleimide group, were detected for PPX-maleimide before

the tape was removed as indicated in Figure 3-3. The results from the IRRAS analysis

from the cross-cut tape test clearly support the highest adhesion strength rating (5B) for

PPX-alkene and PPX-maleimide.

3.1.4 Thermal Stability

The thermal stability of PPX-alkene and PPX-maleimide was tested using IRRAS

analysis as a function of temperature, ranging from 25 °C to 200 °C. The Figure 3-4

revealed that PPX-alkene is thermally stable up to 150 °C and is prone to undergo

compositional changes above this temperature. On the other hand, the data showed PPX-

maleimide is stable up to 100 °C, and then has a tendency to undergo compositional changes. Nevertheless, PPX-alkene and PPX-maleimide both showed stable performance during the temperature range that was sufficient for normal biotechnological uses.
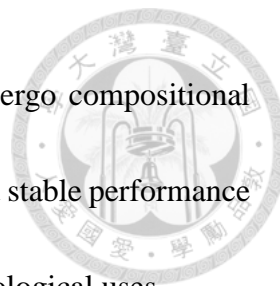
3.1.5 Adherent Property on Bone Plate/Screw Device

The excellent adherent property and coating fidelity was further examined on a Ti6Al4V bone plate/screw device, which is a device subjected to high mechanical shear stress during its locking and unlocking process of operation. A control experiment was first conducted by purposefully creating scratches using a razor blade on a thread region of a PPX-maleimide-deposited screw. These scratches formed flaking lines (approximately 5–10 μm) of scratches, and scattered pieces of coating debris were clearly identified in the SEM image shown in Figure 3-5(a). By contrast, a separate screw (also coated with PPX-maleimide) operated using a normal lock/unlock process was recorded by SEM, and the images were compared before and after the lock/unlock process, showing no change on the surface morphology and no signs of scratches or debris on the coatings, as illustrated in Figure 3-5(a)-(b). These results demonstrate sufficient coating stability against mechanical operation processes by using the reported coatings, and the concern that was raised regarding the coating adhesion to devices, such as bone plates, during the locking/unlocking process is alleviated.[55]
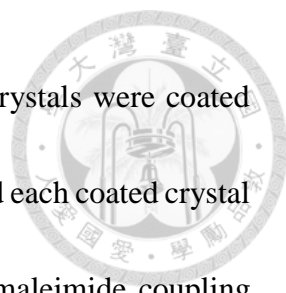
27

3.2 Protein Adsorption

3.2.1 Bioconjugation of CREDV Peptide

Specific conjugation using PPX-alkene to immobilize thiol-terminated molecules, such as with the cysteine-containing peptide, Cys-Arg-Glu-Asp-Val (CREDV), was further verified using IRRAS analysis. Gold substrates were first coated with PPX-alkene via a CVD polymerization process, and subsequently, the CREDV peptide was react with the resulting surface through a photochemically activated thiol-ene click reaction.[31] The IRRAS spectra of the resulting sample in Figure 3 have indicated that characteristic peaks at 1552 cm^{-1} and 1606 cm^{-1} (–C(= O)NH–), 3207 cm^{-1} (–OH), and 3484 cm^{-1} (–NH), attributed to the characteristic absorption bands of CREDV peptide, were detected in both samples before and after the cross-cut tape test. The results confirmed (i) the availability and reactivity of vinyl group on PPX-alkene were able to immobilize thiol-terminated molecule such as a CREDV peptide; and (ii) strong adhesion of the coatings and that the molecules are firmly attached to the coating.

3.2.2 QCM analysis

QCM analysis is a relatively simple procedure and a portable sensor system that can be used to monitor real-time protein adsorption.[56] In this study, we used QCM to further quantify the adsorption behavior of bovine serum albumin (BSA) on coated surfaces that

were immobilized with PEG molecules. In the experiment, QCM crystals were coated

with PPX-alkene and PPX-maleimide using CVD polymerization, and each coated crystal

was subsequently modified with thiol-terminated PEG via a thiol-maleimide coupling

reaction or a thiol-ene click reaction, respectively. The change in the frequency for the

QCM crystal was monitored, while a BSA solution was passed over the crystal surfaces.

The mass adsorbed onto the surface can be quantified from the frequency change

according to the Sauerbrey relationship, where the adsorbed mass is proportional to the

frequency change.[57] As shown in Figure 3-6, the BSA adsorption curves were recorded

for the PEG-modified surfaces on PPX-alkene and PPX-maleimide, and the curves are

compared with control surfaces that were modified with bare PPX-alkene and PPX-

maleimide. High fouling levels were observed for the control surfaces that were barely

coated with PPX-alkene and PPX-maleimide due to a relatively high hydrophobicity, with

a water contact angle of approximately 93 ± 3 degrees for PPX-alkene and 95 ± 2

degrees for PPX-maleimide. For samples coated with PPX-alkene, a 67.6 ± 5.1 Hz

average frequency was observed, which corresponds to a sur- face BSA concentration of

approximately 334.1 ± 25.2 ng cm^{-2}, whereas an average of 64.4 ± 4.8 Hz ($318.2 \pm$

23.7 ng cm^{-2}) was found for PPX-maleimide. In contrast, surfaces modified with PEG

molecules showed significantly lower BSA adsorption with average fre- quencies of 5.0

± 1.1 Hz (24.7 ± 5.4 ng cm^{-2}) and 1.9 ± 0.8 Hz (9.8 ± 3.9 ng cm^{-2}) for PPX-alkene

29

and PPX-maleimide, respectively. Such values clearly support the attachment of PEG

molecules PPX-alkene and PPX-maleimide, a modification that is straightforward and

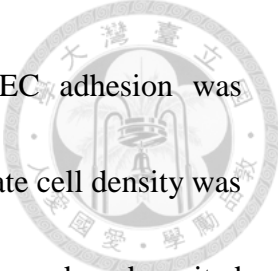provides effective protein resistance.

3.3 Cell Viability

3.3.1 Immobilization of the CREDV Peptide via Click Reaction

We then evaluated the immobilization of the CREDV peptide via click reaction and assessed cell growth in the presence of the immobilized peptide. The REDV peptide is a well-studied cell adhesion motif present in a segment of fibronetin, which is one of the major extracellular matrix proteins. This peptide has been reported to be the minimal active sequence responsible for biding of the region of integrin alpha 4 beta 1 receptor on the endothelial cell.[58] Preferentially attracted binding of human umbilical vein endothelial cells (HUVEC) by using CREDV has also been demonstrated.[59] The cysteine-containing design of CREDV allows this peptide to be orthogonally immobilized by a maleimide or an alkene group via a thiol-maleimide coupling reaction or a thiol-ene click reaction.[31, 32, 60] The CREDV peptide was employed in this study and was immobilized on SS surfaces coated with PPX-alkene and PPX-maleimide. HUVECs were subsequently cultured on the modified surfaces along with another control surface.
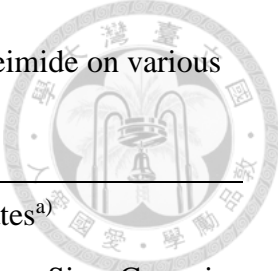
3.3.2 MTT Reduction Assay

We adapted a highly efficient MTT reduction assay to examine the cell activity on treated surfaces, including those with PEG-passivation, bare SS, as-deposited PPX-alkene, as-deposited PPX-maleimide, CREDV-immobilized PPX-alkene, and CREDV-

31

immobilized PPX-maleimide. As indicated in Figure 3-7, HUVEC adhesion was significantly enhanced by the presence of REDV. By contrast, moderate cell density was found on some surfaces, including bare SS, as-deposited PPX-alkene, and as-deposited PPX-maleimide, which lacked the presence of REDV. At last, the attachment and growth of HUVEC was significantly suppressed on the PEG-passivated surface, which clearly sup- ports the fact that the orthogonally immobilized PEG molecules can effectively reduce the effects of fouling substances such as proteins (from the QCM analysis in the previous section) or non-specific cell attachments.[61] A designable coating technology provides (i) a facile surface modification approach, regardless of the underlying substrate materials (SS is selected as example in this case); and (ii) a surface property design using thiol-reactive PPX-alkene and PPX-maleimide to attach a tailored thiol molecule that can be used for immobilizations via a thiol-maleimide coupling reaction or a thiol-ene click reaction that is highly regioselective and rapid.

Table 3-1 Cross-cut tape adhesion test of PPX-alkene and PPX-maleimide on various substrates.

	ASTM D3359 adhesion strength of coatings on substrates[a]								
	Ti6Al4V	Au	SS	PMMA	PS	PC	Glass	Si	Ceramic
PPX-alkene	5B	5B	5B	5B	5B	5B	5B	5B	5B
PPX-maleimide	5B	5B	5B	5B	5B	5B	5B	5B	5B

[a]ASTM D3359 classification of adhesion strength. (5B): the edges of the cuts are completely smooth; none of the squares or the lattice are detached; (4B): less than 5% of the latticed area is detached; (3B): 5 to 15% of the lattice is detached; (2B): 15 to 35% of the lattice is detached; (1B): 35 to 65% of the lattice is detached; (0B): flaking and detachment in excess of 65%.
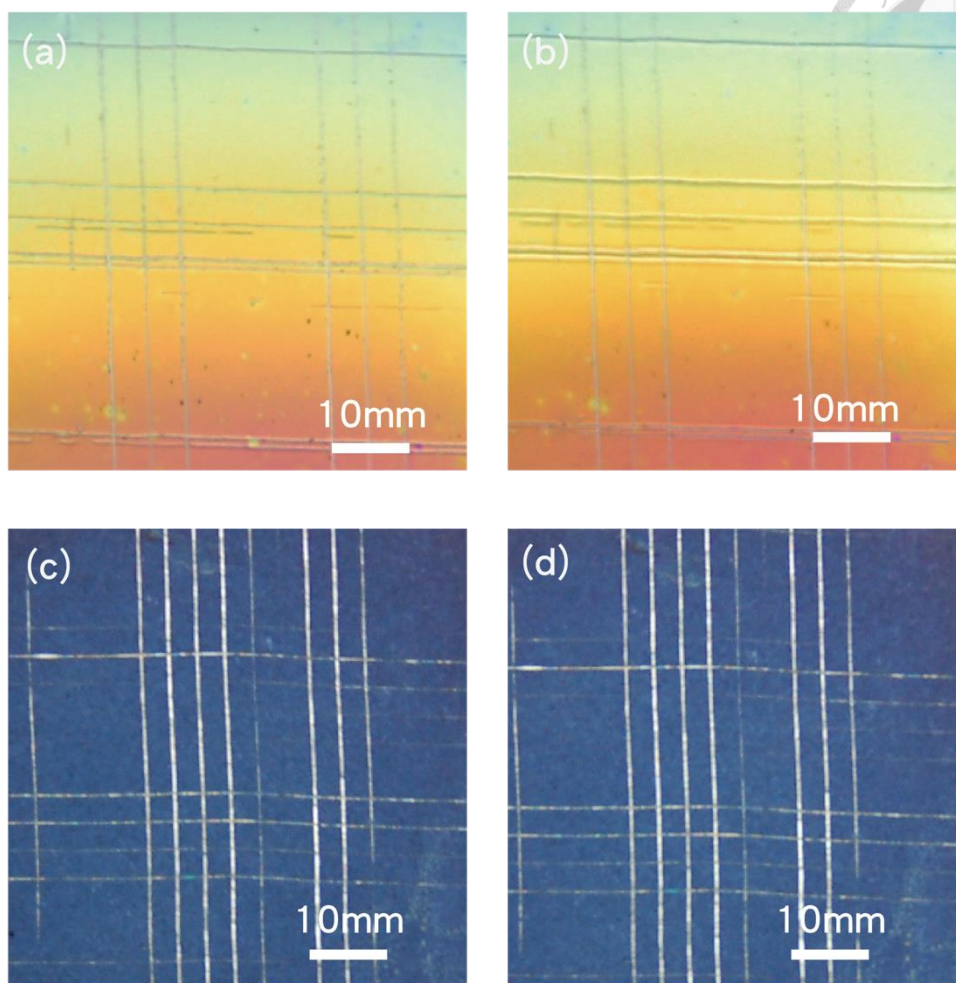
Figure 3-1 Images of cross-cut tape adhesion test on substrates that were modified with PPX-alkene and PPX-maleimide.
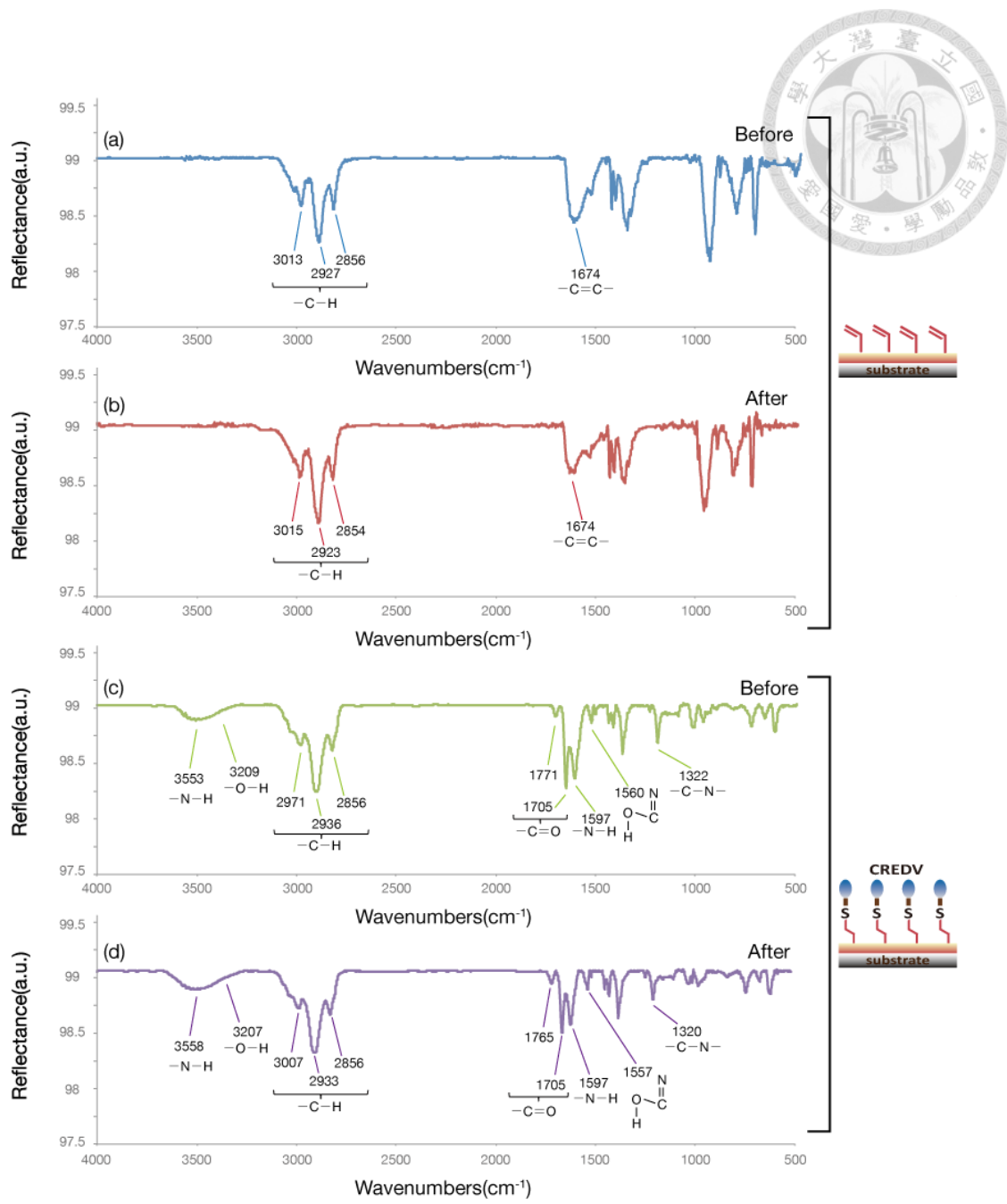
Figure 3-2 IRRAS characterizations of as-deposited PPX-alkene.

Figure 3-3 IRRAS characterizations of as-deposited PPX-maleimide.

Figure 3-4 IRRAS characterizations to test thermal stability of PPX-alkene.

37

Figure 3-5 SEM micrographs of a PPX-maleimide-deposited bone screw.

Figure 3-6 QCM analysis of adsorbed BSA proteins on different surfaces.

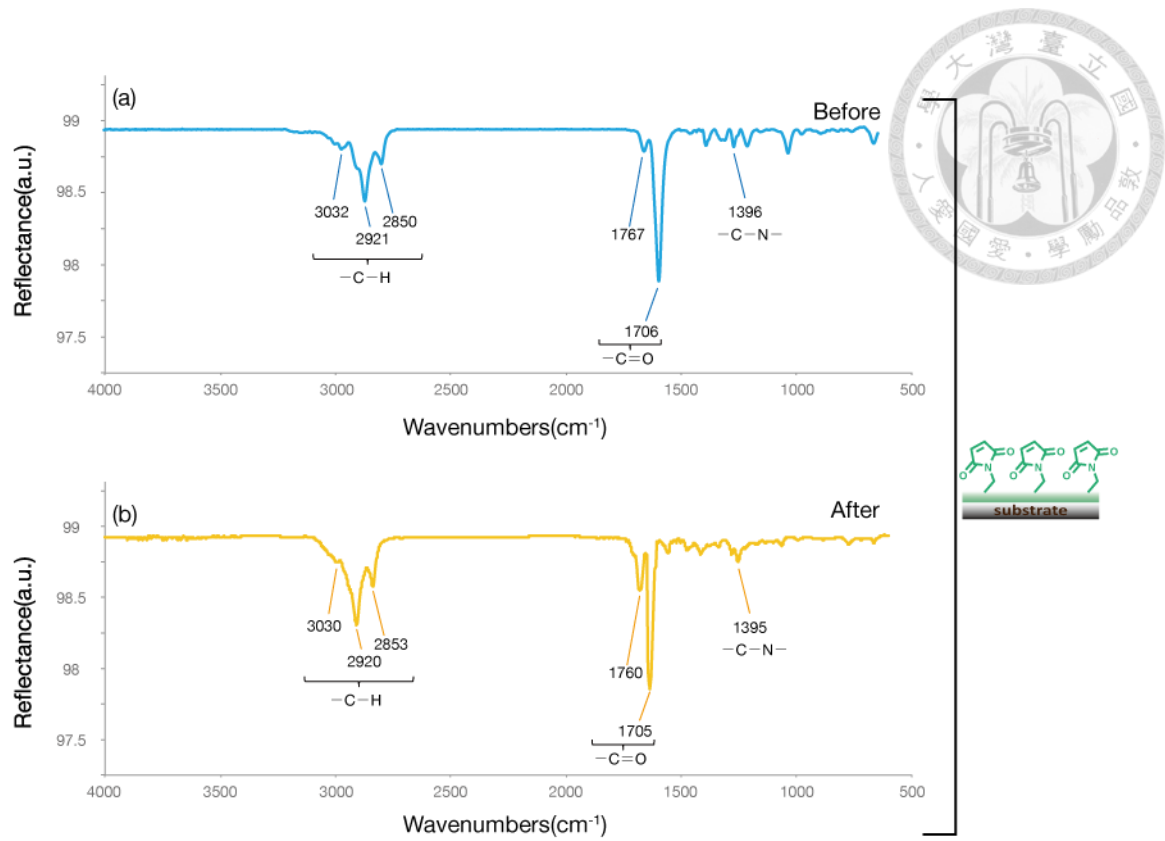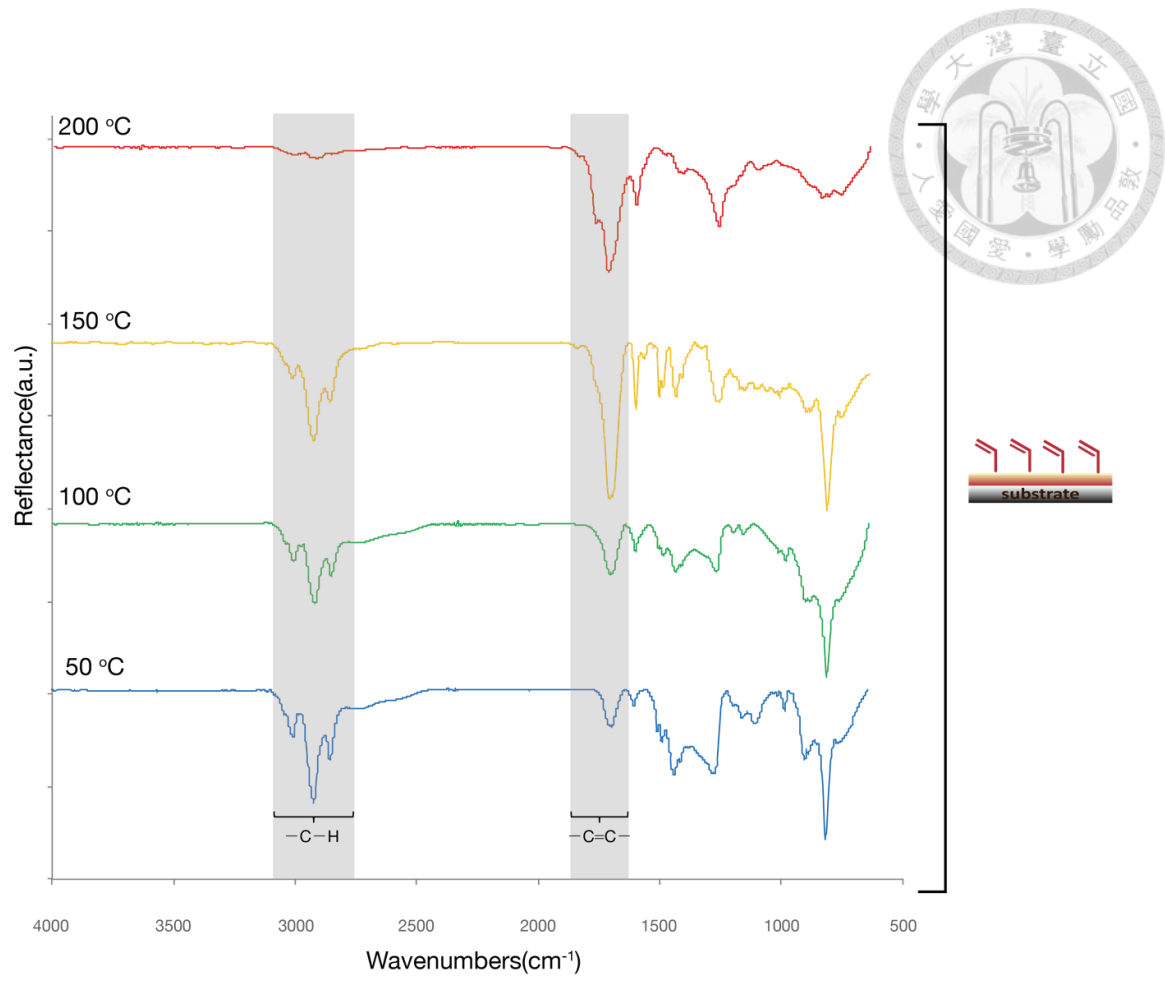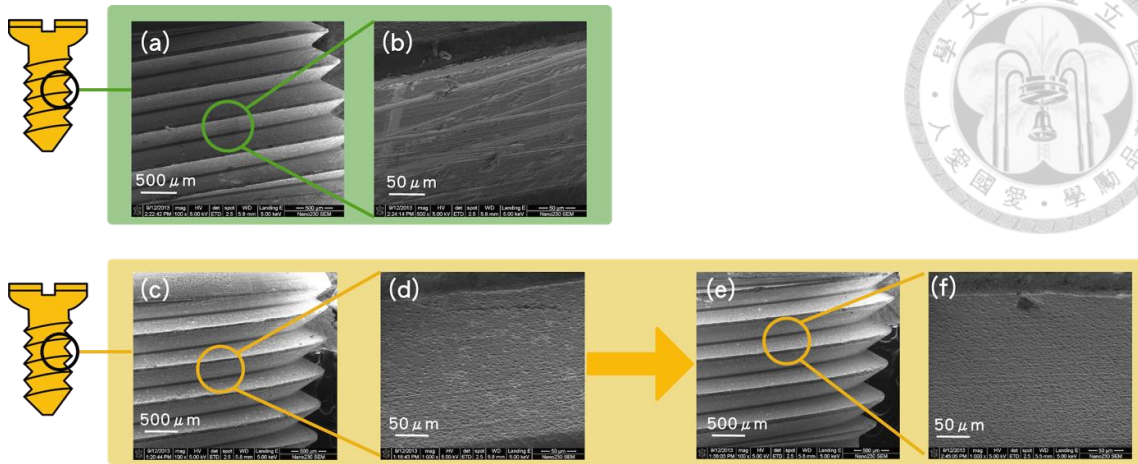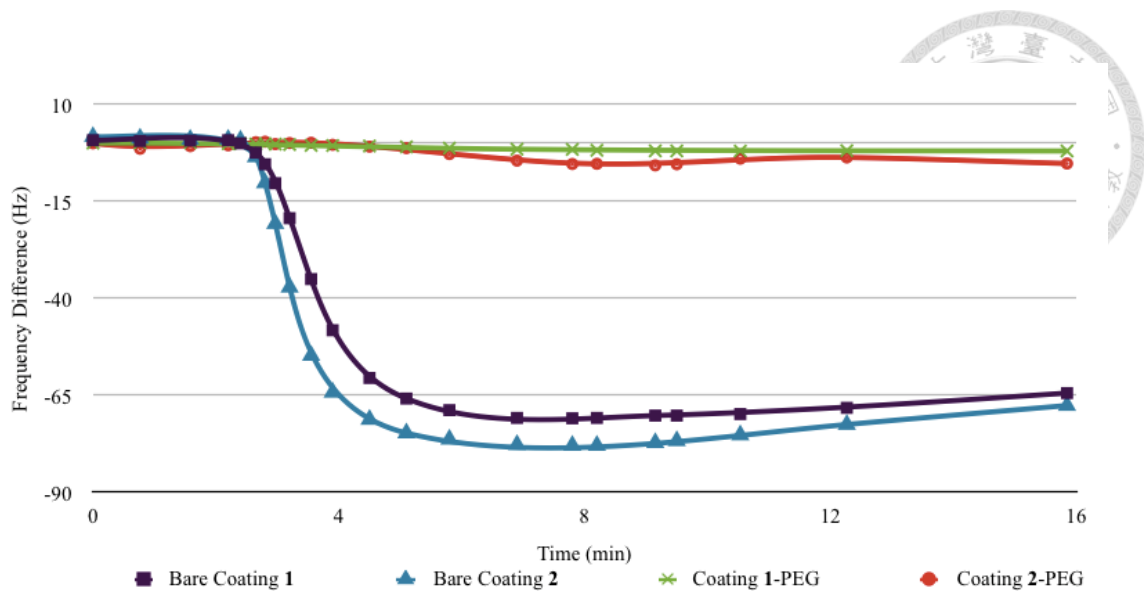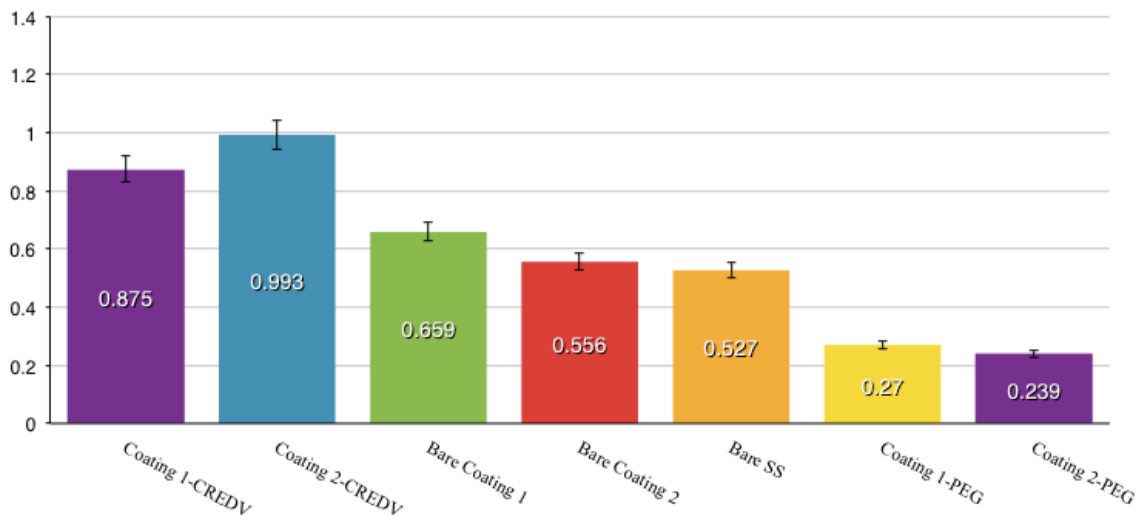Figure 3-7 HUVEC cell viability assessed by MTT reduction assay on surfaces with different modification conditions.

Chapter 4 Selective Deposition

4.1 Surface Inhibition

Several transition metals, such as iron, copper, silver, and platinum, have been shown in previous reports to provide high surface energy for the neutralization of quinodimethanes on the substrate surface and prevent further initiation and propagation of the polymerization reaction from forming PPXs.[47] Limitations of the selective deposition were found only for nonfunctional PPXs and vinyl-functionalized PPXs on a small group of metal surfaces. Other functionalized PPXs showed a higher interaction with the underlying substrates and demonstrated no inhibition regardless of the high surface energy of certain transition metals.[48] In light of these outcomes and considering that the high surface energy of these substrates may account for the neutralization of quinodimethanes, we herein hypothesized that supplying electrical energy to the substrate surface can enhance deposition selectivity by increasing the transition of the surface energy instead of relying on the innate and native surface energy of the substrates. The approach of charging the substrate surface is as following,

a. Universally applicable to other conducting substrates

b. Demonstrates effective selectivity for the deposition of both nonfunctional PPXs

and the family of functionalized PPXs.

The evidence for deposition selectivity was first verified by using IRRAS. The

spectra were recorded and compared with the surfaces after the CVD deposition of PPX-

C or PPX-aldehyde on titanium (Ti), copper (Cu), silver (Ag), gold (Au), zinc (Zn),

aluminium (Al), and conducting glasses with fluorine-doped SnO_2 (FTO), where

electrical charges were applied to the substrates. Control substrates without applied

charges were also tested in parallel for comparison. As indicated in Fig 4-1 a-b, the spectra

were dominated by characteristic –C–Cl stretching at 1030-1100 cm^{-1} for PPX-C (Fig 4-

1a), at 2860-3040 cm^{-1} for the symmetric and asymmetric stretching corresponding to –

C–H absorptions, and at approximately 1662 and 1603 cm^{-1} attributed to unsaturated –

C=O stretching for PPX-aldehyde, as demonstrated in (Fig 4-1b). These characteristic

bands were present on the pure substrate surfaces and showed consistent selectivity

compared with previous reported results.[47, 48] In contrast, all these bands could not be

observed on the same metals or FTO substrates with the addition of applied electrical

charges (Fig 4-1 c-d). These results revealed that a universal selectivity was found for

conducting substrates and that the selectivity was equally applicable for both

42

nonfunctional and functionalized PPXs. The same approach described for PPX-C and

PPX-aldehydes was then applied to other PPXs, including PPX-TFA and PPX-amine, on

the same selection of conducting substrates, and the results are recorded in Fig 4-2.
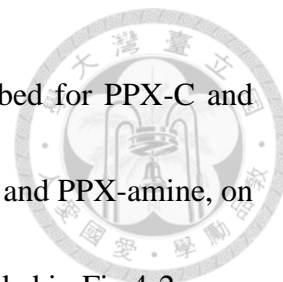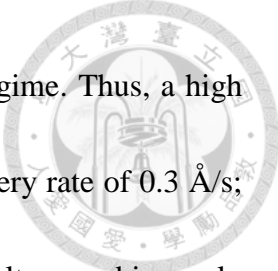
4.2 Selective Deposition Thickness

4.2.1 Maximum Deposition Thickness with Varying Charging Intensities

The existence of an upper limit, i.e., a maximum deposition thickness of PPX, at which deposition will commence and the relative selectivity of the charged surface will be lost, was examined on Al substrates, which previously showed no inhibitory effect for PPXs.[47] As indicated in Fig. 4-3a, a selectivity loss eventually occurred after the deposition of thick PPX-C or PPX-aldehyde (by comparison with a reference surface without applied electrical charges), and a tendency of increased electrical energy was found to be correlated to a greater inhibitor surface (thicker maximum deposition thickness). This trend was also anticipated for all the PPX studied, irrespective of their substituted functionalities. The results of varying the monomer delivery rate as a function of the maximum deposition thickness on such charged surfaces supported the previously found deactivation theory.[47]

4.2.2 Maximum Deposition Thickness with Varying Deposition Rates

The reported rate equation was found to correlate well with the deposition of the studied PPX-C or PPX-aldehyde on the charged surfaces (Fig 4-3b). Furthermore, compared with the native activity of transition metals (literature data shown in Fig 4-3b), the higher activity provided by the charged surfaces resulted in a shift in the required

44

selective deposition conditions in the low monomer delivery rate regime. Thus, a high

maximum deposition thickness can be reached with a very low delivery rate of 0.3 Å/s;

such control was previously thought to be impossible.[47] These results unambiguously

support our hypothesis of an augmented transition of the surface energy to the substrates,

thereby serving as a better inhibitor of the deposition of PPXs. This active pathway is

anticipated to be applicable to other conducting substrates.

4.3 Patterned Substrates

Patterned substrates were prepared by placing conducting Al metal channels on a nonconductive glass surface and allowing for the selective deposition of PPX-TFA, PPX-amine, and PPX-aldehyde. SEM image in Fig 4-4a shows the deposition footprint of the selectively deposited PPX-aldehyde on the anticipated areas of glass background, where no charged was applied. Furthermore, EDS elemental mapping analysis revealed the selective growth of these PPXs films by showing a spatially confined distribution of fluorine signals for PPX-TFA, nitrogen signals for PPX-amine, oxygen signals for PPX-aldehyde, and chlorine signals for PPX-C (Fig 4-4b-e). These fluorine-, nitrogen-, oxygen- and chlorine-containing areas unambiguously correspond to the negative areas of patterned Al (verified Al elemental map shown in Fig 4-4f), providing direct evidence that these PPXs were inhibited by the electrically charged Al surfaces during CVD polymerization. The resulting patterned polymer film of PPX-aldehyde also showed reactive characteristics to support nucleophilic addition with a hydrazine or hydrazide to yield hydrazones.[62] Fluorescently labelled Alexa Fluor® 568 hydrazide molecules were allowed to react with the aldehyde side groups on PPX-aldehyde, and the fluorescence signals were only detected on those areas in which the Al/electrically charged characteristics were absent, as indicated in Fig 4-4g. These results unambiguously verify that the growth of the functional PPX-aldehyde was inhibited by such a charged surface.

46
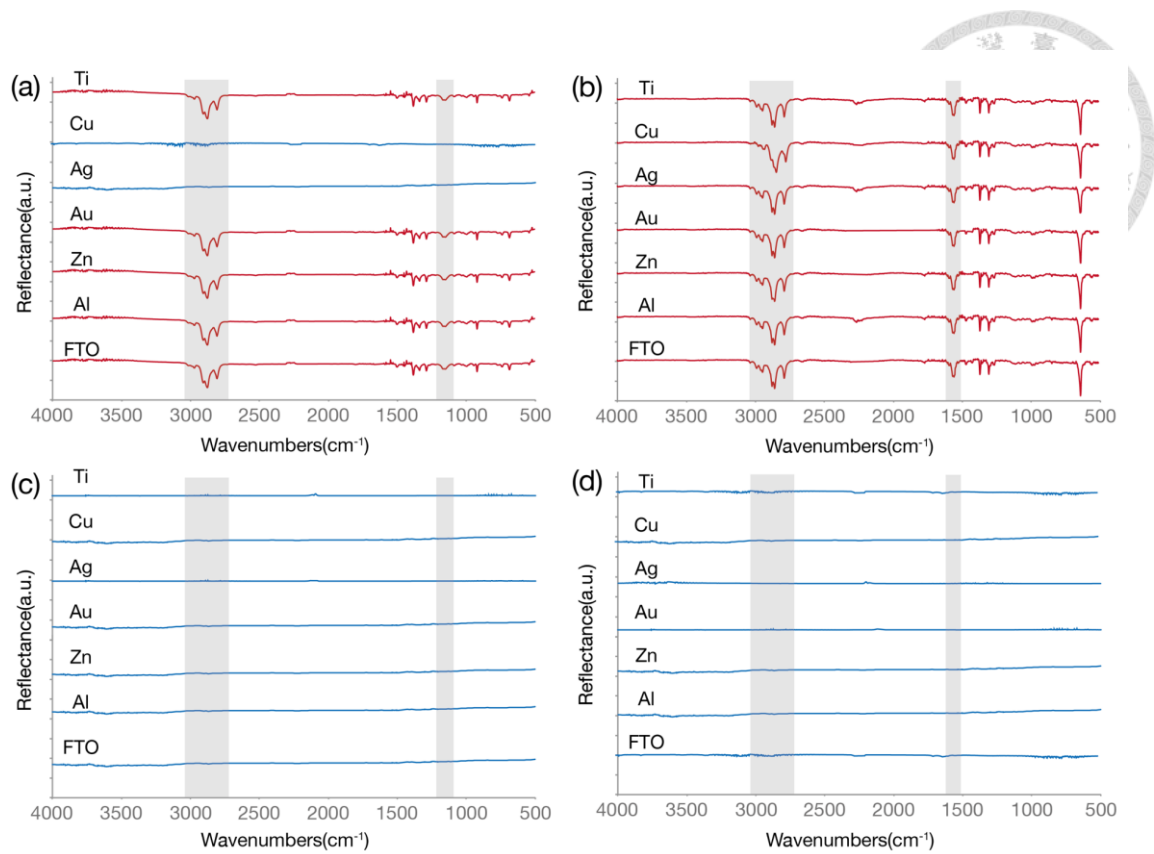
Fig 4-1 IRRAS characterizations of selectively deposited PPX-C and PPX-aldehyde on different conducting substrates.
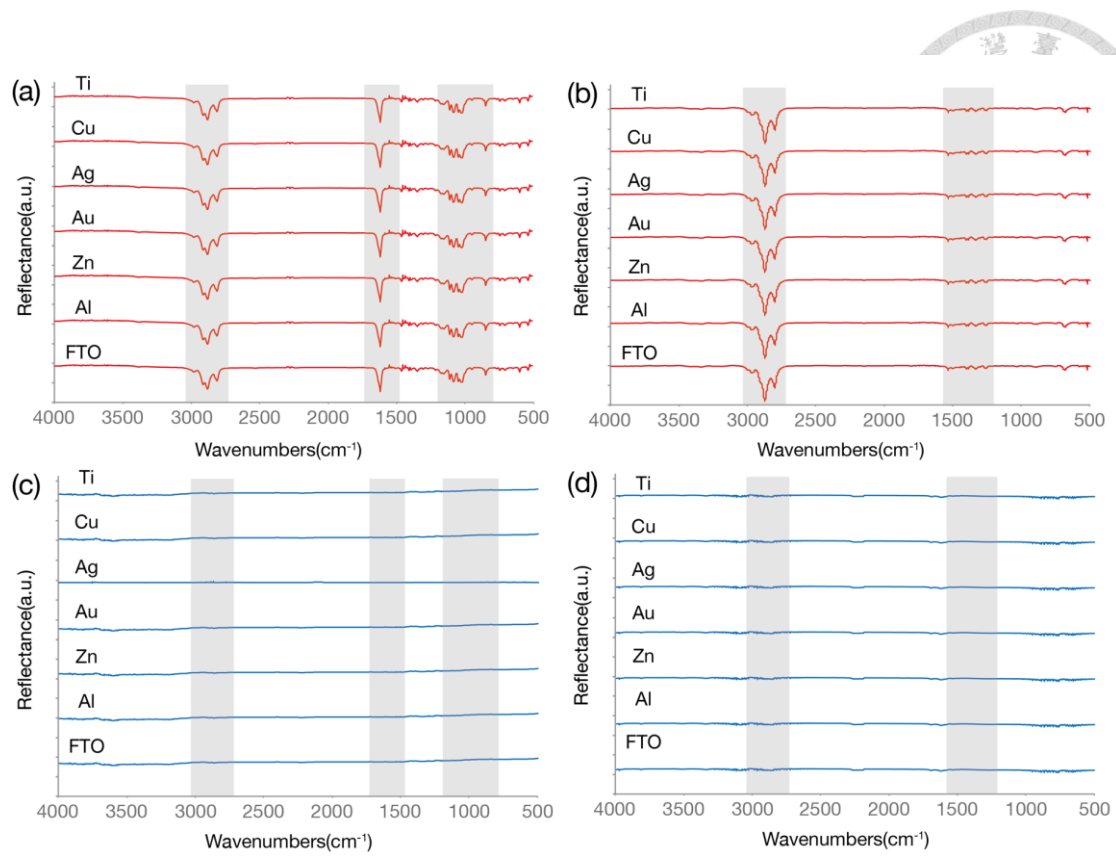
Fig 4-2 IRRAS characterizations of selectively deposited PPX-TFA and PPX-amine on different conducting substrates.
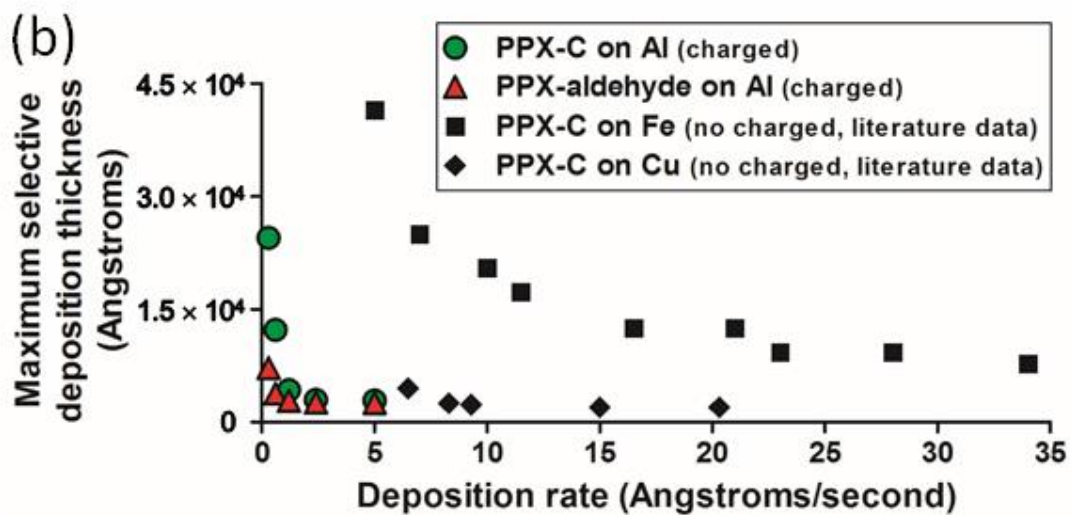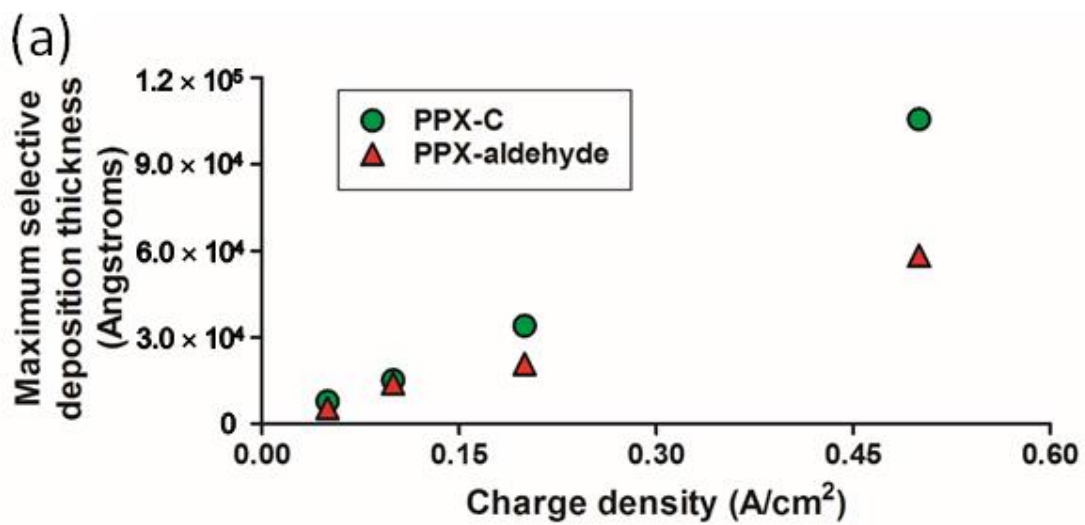
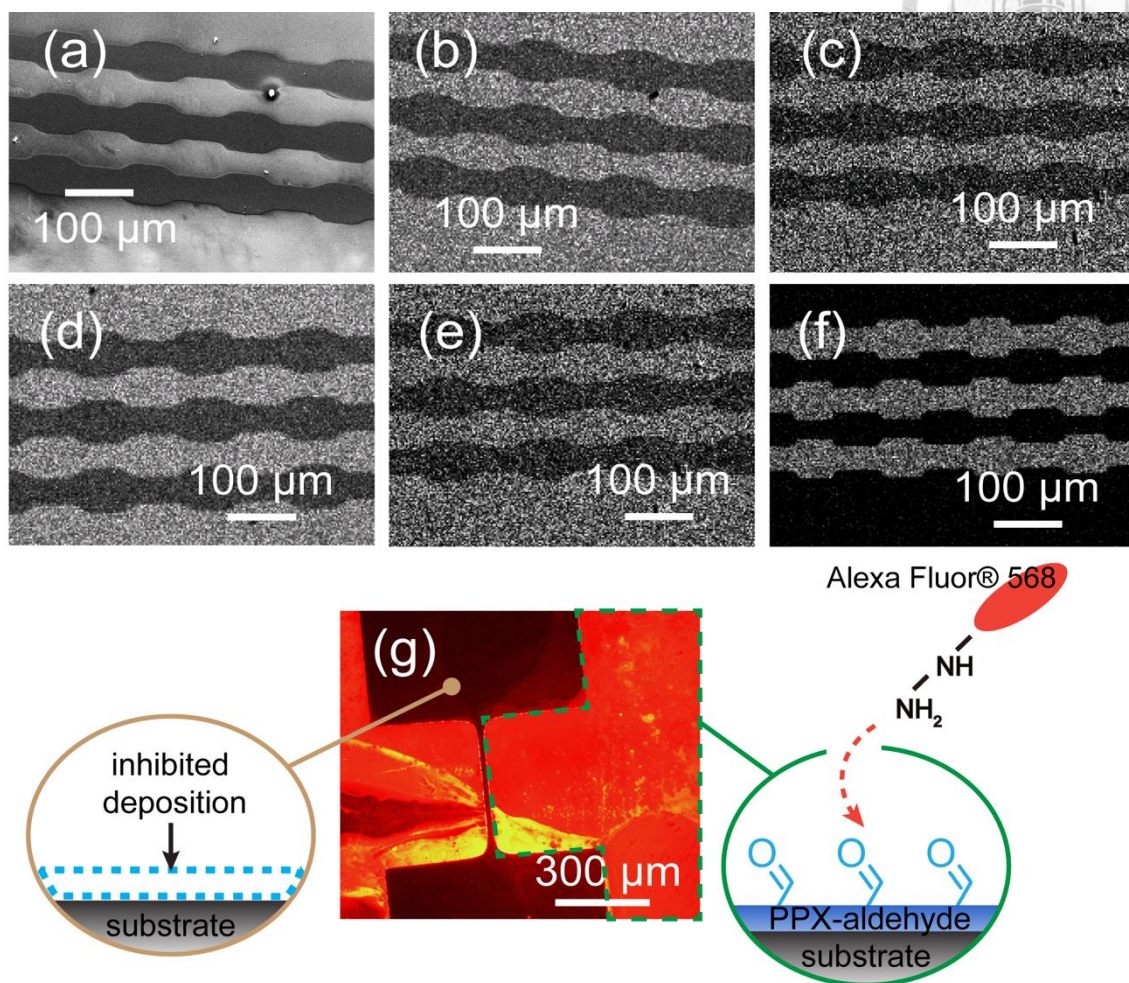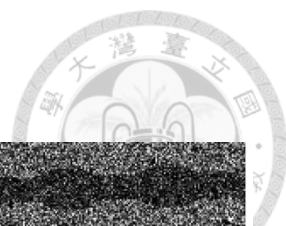Fig 4-3 Maximum selective deposition thickness of PPX-C and PPX-aldehyde on charged Al substrates.

Fig 4-4 Selective deposition of PPX-TFA, PPX-amine, PPX-aldehyde, and PPX-C on patterned substrates of Al.

Chapter 5 Conclusions

5.1 Conclusions

In summary, the parylene coatings with excellent thermal stability and a robust cohesive property against various substrate materials were introduced in this study. All of these coatings achieved Grade 5B adhesion strength on the selected materials tested according to ASTM D3359. Furthermore, the remarkable adhering property and coating fidelity was also successfully demonstrated during the locking and unlocking process for a bone plate/bone screw device, where both properties are indeed required for such a device. In addition, designed surface properties can be tailored through immobilizing thiol-molecules via specific conjugation reaction, such as a thiol-ene click reaction or a thiol–maleimide coupling reaction. Biofunctional surfaces with suppressed protein fouling and enhanced surface affinity toward endothelial cell attachment were demonstrated in the study. As prospective materials require more delicate and sophisticated functions on their surfaces, together with the fabrication of miniature-sized devices with complicated geometries, control over the surface properties requires precision in both the chemical and topological definitions with respect to the spatial resolution and chemical functionalities. The introduced selective deposition technology is not constrained to nonfunctional PPX-C or to vinyl-functionalized PPXs, which were

51

found to selectively deposit only on transition metals. In addition, this technology

provides a simple and robust tool to modify material surfaces from the bottom up. The

vapour-based deposition characteristics also feature a general method through which the

coating can be prepared conformally with respect to substrate topology, curvature, and

geometry, and the deposition and immobilization technologies of PPXs are well-

transferred from one substrate to another.[63, 64]
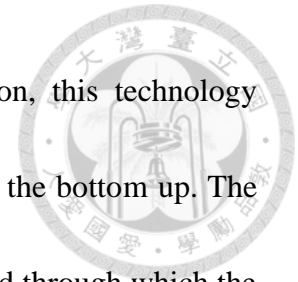
5.2 Future Works

The coating technology reported allow for facile and versatile surface modification, although limited to related applications and devices shown in the study and is however expected to extend to surface applications that require sophisticated property designs and complicated device geometries. In addition, dedicated to the manipulation of the electrical parameters, the determination of the critical thickness on different conducting materials (including metals, indium tin oxide and their derivatives and wide selections of conducting polymers and graphene), and the multifunctional presentation of selectively deposited PPXs with distinct functionalities. The extension of the selective deposition technology can transfer well from the reported functionalities to other existing libraries of functional PPXs.[24, 36, 65] We foresee the use of this technology for the development of next-generation implantable devices, cellular assays, tissue engineering, and regenerative medicine applications.

53

Reference
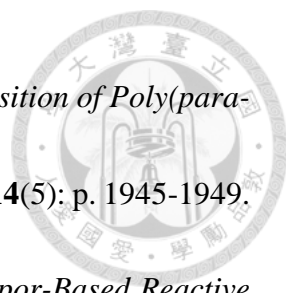
1. Banerjee, I., R.C. Pangule, and R.S. Kane, *Antifouling coatings: recent developments in the design of surfaces that prevent fouling by proteins, bacteria, and marine organisms.* Adv Mater, 2011. **23**(6): p. 690-718.

2. Shin, H., S. Jo, and A.G. Mikos, *Biomimetic materials for tissue engineering.* Biomaterials, 2003. **24**(24): p. 4353-4364.

3. Castner, D.G. and B.D. Ratner, *Biomedical surface science: Foundations to frontiers.* Surface Science, 2002. **500**(1–3): p. 28-60.

4. Stevens, M.M. and J.H. George, *Exploring and engineering the cell surface interface.* Science, 2005. **310**(5751): p. 1135-1138.

5. von der Mark, K., et al., *Nanoscale engineering of biomimetic surfaces: cues from the extracellular matrix.* Cell and Tissue Research, 2010. **339**(1): p. 131-153.

6. Jensen, U.B., S. Lowell, and F.M. Watt, *The spatial relationship between stem cells and their progeny in the basal layer of human epidermis: a new view based on whole-mount labelling and lineage analysis.* Development, 1999. **126**(11): p. 2409-2418.

7. Darouiche, R.O., *Treatment of Infections Associated with Surgical Implants.* New England Journal of Medicine, 2004. **350**(14): p. 1422-1429.
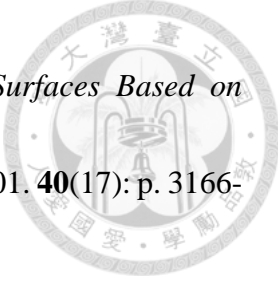
8. Norowski, P.A. and J.D. Bumgardner, *Biomaterial and antibiotic strategies for peri-implantitis: A review.* Journal of Biomedical Materials Research Part B: Applied Biomaterials, 2009. **88B**(2): p. 530-543.

9. Eisenberg, M.J. and K.J. Konnyu, *Review of Randomized Clinical Trials of Drug-Eluting Stents for the Prevention of In-Stent Restenosis.* The American Journal of Cardiology, 2006. **98**(3): p. 375-382.

10. Lewis, F. and D. Mantovani, *Methods to Investigate the Adhesion of Soft Nano-Coatings on Metal Substrates – Application to Polymer-Coated Stents.* Macromolecular Materials and Engineering, 2009. **294**(1): p. 11-19.

11. Luo, Y., et al., *The friction and wear behavior of WC coating on medical grade titanium alloys.* Proceedings of the Institution of Mechanical Engineers, Part J: Journal of Engineering Tribology, 2013. **227**(8): p. 845-849.

12. Sun, T., et al., *Functional biointerface materials inspired from nature.* Chem. Soc. Rev., 2011. **40**(5): p. 2909-2921.

13. Cole, M.A., et al., *Stimuli-responsive interfaces and systems for the control of protein–surface and cell–surface interactions.* Biomaterials, 2009. **30**(9): p. 1827-1850.

14. Geiger, B., J.P. Spatz, and A.D. Bershadsky, *Environmental sensing through focal adhesions.* Nat. Rev. Mole. Cell Biol., 2009. **10**(1): p. 21-33.

15. Sniadecki, N.J., et al., *Magnetic microposts as an approach to apply forces to living cells.* Proc. Natl. Acad. Sci. U.S.A., 2007. **104**: p. 14553-14558.

16. Dalby, M.J., et al., *Use of nanotopography to study mechanotransduction in fibroblasts - methods and perspectives.* Eur. J. Cell Biol., 2004. **83**(4): p. 159-169.

17. Nie, Z. and E. Kumacheva, *Patterning surfaces with functional polymers.* Nat. Mater., 2008. **7**(4): p. 277-290.

18. Biswas, A., et al., *Advances in top–down and bottom–up surface nanofabrication: Techniques, applications & future prospects.* Adv. Coll. Inter. Sci., 2012. **170**(1–2): p. 2-27.

19. Lu, W. and C.M. Lieber, *Nanoelectronics from the bottom up.* Nat. Mater., 2007. **6**(11): p. 841-850.

20. Hauser, C.A.E. and S. Zhang, *Designer self-assembling peptide nanofiber biological materials.* Chem. Soc. Rev., 2010. **39**(8): p. 2780-2790.

21. Kramer, P., et al., *Polymerization of para-xylylene derivatives (parylene polymerization). I. Deposition kinetics for parylene N and parylene C.* Journal of Polymer Science: Polymer Chemistry Edition, 1984. **22**(2): p. 475-491.

22. Wu, P., et al., *Deposition of High Purity Parylene- F Using Low Pressure Low Temperature Chemical Vapor Deposition.* Journal of Electronic Materials, 1997. **26**(8): p. 949-953.

23. Fortin, J.B. and T.M. Lu, *A Model for the Chemical Vapor Deposition of Poly(para-xylylene) (Parylene) Thin Films.* Chemistry of Materials, 2002. **14**(5): p. 1945-1949.

24. Chen, H.-Y. and J. Lahann, *Designable Biointerfaces Using Vapor-Based Reactive Polymers.* Langmuir, 2010. **27**(1): p. 34-48.

25. Naddaka, M., et al., *Functionalization of parylene during its chemical vapor deposition.* Journal of Polymer Science Part A: Polymer Chemistry, 2011. **49**(13): p. 2952-2958.

26. Yang, R., A. Asatekin, and K.K. Gleason, *Design of conformal, substrate-independent surface modification for controlled protein adsorption by chemical vapor deposition (CVD).* Soft Matter, 2012. **8**(1): p. 31-43.

27. Chen, H.-Y., et al., *Colloids with high-definition surface structures.* Proceedings of the National Academy of Sciences, 2007. **104**(27): p. 11173-11178.

28. Nandivada, H., et al., *Reactive Polymer Coatings that "Click".* Angewandte Chemie International Edition, 2006. **45**(20): p. 3360-3363.

29. Katira, P., et al., *Quantifying the Performance of Protein-Resisting Surfaces at Ultra-Low Protein Coverages using Kinesin Motor Proteins as Probes.* Advanced Materials, 2007. **19**(20): p. 3171-3176.

30. Chen, H.-Y. and J. Lahann, *Preparation of Non-Fouling Coatings Made by Chemical Vapor Deposition Polymerization.* Polymer Preprints, 2005.

31. Wu, J.-T., et al., *Reactive Polymer Coatings: A General Route to Thiol-ene and Thiol-yne Click Reactions.* Macromolecular Rapid Communications, 2012. **33**(10): p. 922-927.

32. Tsai, M.-Y., et al., *Vapor-based synthesis of maleimide-functionalized coating for biointerface engineering.* Chemical Communications, 2012. **48**(89): p. 10969-10971.

33. Chen, H.-Y., et al., *Vapor-based tri-functional coatings.* Chemical Communications, 2013. **49**(40): p. 4531-4533.

34. Elkasabi, Y., et al., *Towards Multipotent Coatings: Chemical Vapor Deposition and Biofunctionalization of Carbonyl-Substituted Copolymers.* Macromolecular Rapid Communications, 2008. **29**(11): p. 855-870.

35. Elkasabi, Y., H.-Y. Chen, and J. Lahann, *Multipotent Polymer Coatings Based on Chemical Vapor Deposition Copolymerization.* Advanced Materials, 2006. **18**(12): p. 1521-1526.

36. Lahann, J. and R. Langer, *Novel Poly(p-xylylenes): Thin Films with Tailored Chemical and Optical Properties.* Macromolecules, 2002. **35**(11): p. 4380-4386.

37. Seymour, J.P., et al., *The insulation performance of reactive parylene films in implantable electronic devices.* Biomaterials, 2009. **30**(31): p. 6158-6167.

38. Lahann, J., et al., *Reactive Polymer Coatings: A First Step toward Surface Engineering of Microfluidic Devices.* Anal. Chem., 2003. **75**(9): p. 2117-2122.

39. Lahann, J., et al., *A New Method toward Microengineered Surfaces Based on Reactive Coating.* Angewandte Chemie International Edition, 2001. **40**(17): p. 3166-3169.

40. Chen, H.-Y. and J. Lahann, *Vapor-Assisted Micropatterning in Replica Structures: A Solventless Approach towards Topologically and Chemically Designable Surfaces.* Adv. Mater., 2007. **19**(22): p. 3801-3808.

41. Chen, H.-Y. and J. Lahann, *Fabrication of Discontinuous Surface Patterns within Microfluidic Channels Using Photodefinable Vapor-Based Polymer Coatings.* Anal. Chem., 2005. **77**(21): p. 6909-6914.

42. Sun, H.-Y., et al., *Thiol-Reactive Parylenes as a Robust Coating for Biomedical Materials.* Adv. Mater. Inter., 2014. **1**(6): p. 1400093.

43. Chen, H.-Y., et al., *Colloids with high-definition surface structures.* Proc. Natl. Acad. Sci., 2007. **104**(27): p. 11173-11178.

44. Wu, M.-G., et al., *Vapor-Deposited Parylene Photoresist: A Multipotent Approach toward Chemically and Topographically Defined Biointerfaces.* Langmuir, 2012. **28**(40): p. 14313-14322.

45. Senkevich, J.J., et al., *Selective deposition of ultrathin poly(p-lxylylene) films on dielectrics versus copper surfaces.* Chemical Vapor Deposition, 2004. **10**(5): p. 247-+.

46. Vaeth, K.M. and K.F. Jensen, *Selective growth of poly(p-phenylene vinylene) prepared bg chemical vapor deposition.* Advanced Materials, 1999. **11**(10): p. 814-820.

47. Vaeth, K.M. and K.F. Jensen, *Transition metals for selective chemical vapor deposition of parylene-based polymers.* Chemistry of Materials, 2000. **12**(5): p. 1305-1313.

48. Chen, H.-Y., et al., *Substrate-Selective Chemical Vapor Deposition of Reactive Polymer Coatings.* Advanced Materials, 2008. **20**(18): p. 3474-3480.

49. D3359-02, A., *Standard Test Methods for Measuring Adhesion by Tape Test.* ASTM International.

50. Iwatsuki, S., et al., *Synthesis and Polymerization of 4-Vinyl [2.2]Paracyclophane.* Polymer Bulletin, 1994. **32**(1): p. 27-34.

51. Gorham, W.F., *A New, General Synthetic Method for the Preparation of Linear Poly-p-xylylenes.* Journal of Polymer Science Part A-1: Polymer Chemistry, 1966. **4**(12): p. 3027-3039.

52. Lewis, F., et al., *Study of the adhesion of thin plasma fluorocarbon coatings resisting plastic deformation for stent applications.* Journal of Physics D: Applied Physics, 2008. **41**(4): p. 045310.

53. Chen, C.-Y., et al., *Low-shrinkage visible-light-curable urethane-modified epoxy*

acrylate/SiO2 composites as dental restorative materials. Composites Science and

Technology, 2008. **68**(13): p. 2811-2817.

54. Kasuya, M., et al., *Quantification of ATRP initiator density on polymer latex particles by fluorescence labeling technique using copper-catalyzed azide-alkyne cycloaddition.* Journal of Polymer Science Part A: Polymer Chemistry, 2013. **51**(19): p. 4042-4051.

55. Fritsche, A., et al., *Mechanical characterization of anti-infectious, anti-allergic, and bioactive coatings on orthopedic implant surfaces.* Journal of Materials Science, 2009. **44**(20): p. 5544-5551.

56. Marx, K.A., *Quartz Crystal Microbalance: A Useful Tool for Studying Thin Polymer Films and Complex Biomolecular Systems at the Solution−Surface Interface.* Biomacromolecules, 2003. **4**(5): p. 1099-1120.

57. Sauerbrey, G., *Verwendung von Schwingquarzen zur Wägung dünner Schichten und zur Mikrowägung.* Zeitschrift für Physik, 1959. **155**(2): p. 206-222.

58. Massia, S.P. and J.A. Hubbell, *Vascular endothelial cell adhesion and spreading promoted by the peptide REDV of the IIICS region of plasma fibronectin is mediated by integrin alpha 4 beta 1.* Journal of Biological Chemistry, 1992. **267**(20): p. 14019-14026.

59. Plouffe, B.D., et al., *Peptide-Mediated Selective Adhesion of Smooth Muscle and*

Endothelial Cells in Microfluidic Shear Flow. Langmuir, 2007. **23**(9): p. 5050-5055.

60. Hoyle, C.E. and C.N. Bowman, *Thiol-Ene Click Chemistry.* Angewandte Chemie-International Edition, 2010. **49**(9): p. 1540-1573.

61. Branch, D.W., et al., *Long-term stability of grafted polyethylene glycol surfaces for use with microstamped substrates in neuronal cell culture.* Biomaterials, 2001. **22**(10): p. 1035-1047.

62. Nandivada, H., H.-Y. Chen, and J. Lahann, *Vapor-Based Synthesis of Poly[(4-formyl-p-xylylene)-co-(p-xylylene)] and Its Use for Biomimetic Surface Modifications.* Macromole. Rapid Comm., 2005. **26**(22): p. 1794-1799.

63. Wu, J.-T., et al., *Reactive Polymer Coatings: A General Route to Thiol-ene and Thiol-yne Click Reactions.* Macromole. Rapid Comm., 2012. **33**(10): p. 922-927.

64. Chen, H.-Y., et al., *Substrate-Independent Dip-Pen Nanolithography Based on Reactive Coatings.* J. Am. Chem. Soc., 2010. **132**(51): p. 18023-18025.

65. Lu, B., et al., *A study of the autofluorescence of parylene materials for [small mu]TAS applications.* Lab Chip, 2010. **10**(14): p. 1826-1834.

口試提問

戴: 通電的概念是甚麼?

ANS: 在 coating 的時候,chamber 接電。

戴: 為什麼你覺得通電的表面會有影響?

ANS: 我們是從過去的研究找到靈感,有的單體遇到活性比較高的金屬時,所以單體碰到高能量表面之後,單體就失去活性了,所以根據這樣的現象,我們嘗試用通電的方式來做。

戴: 所以是因為單體活性較低,讓他不能聚合嗎?

ANS: 因為單體沒有活性,所以不好聚合。

戴: 可不可以讓它反過來,本來不會長,反過來變成會長?

ANS: 我們的通電表面,讓單體無法再表面聚合,但當單體覆蓋表面後,還是會有二次聚合。

戴: 怎麼分辨初次或二次沉積,還有 IR、百格刀,oligomer 會不有影響?

ANS: 通電的聚合,沒有做百格刀測試,但可以做做看,看 oligomer 會不會有影響。

戴: 有沒有任何東西是說,原先不會沉積,但因為會通電,而讓它會沉積?

ANS: 除了某幾個過度金屬之外,目前沒有特別研究不會沉積的表面

戴: 非金屬的通電壓會有甚麼影響?

ANS: 我們主要都是固定電流,然後分金屬通電也沒試過,跟據 paper,過度金屬有較高能量可能會抑制高分子,所以我們用這個概念,通電給他能量,抑制高分子聚合。

戴: Parylene 是很好的防水材質,你知道他的防水效果如何?

ANS: 之前有做過包覆液體,用 Parylene 包覆水,所以 Prylene 是防水的,但 permeability 沒有測試過。

戴: 那 contact angle 如何?

ANS: 基本上它是疏水的，所以 contact angle 蠻大的

戴: 假設沉積在高分子上，adhesion 好嗎?

ANS: 之前有試過 coating 在 PS，蠻好的

戴: 你們有沒有做 coating 在 hydrogel 上?

ANS: 沒有試過。

(開啟一段 hydrogel 多孔性、孔洞、包細胞、組織工程的討論)

戴: 這個材料疏水，那有辦法做出超疏水嗎?

ANS: 大概有做到 150 度過。

戴: 這些官能基對沉積有沒有甚麼影響?

ANS: 對於沉積條件上是類似的，但參數有有所差別。

戴: 為什麼雙鍵不會沉積，其他會沉積，為什麼?

ANS: 鹵素相對於其他非鹵素類的，比較不穩定，所以不太會沉積。

戴: 有沒有機會在 coating 時加入一些無機的東西?

ANS: 沒有嘗試過。

趙: 剛剛是用甚麼基材通電?

ANS: 需要是導體，金屬或 ITO 導電玻璃。

趙: P15 是物理性的，我很好奇，物理百格刀的切，怎麼會擔心傷到 functional group?

ANS: 怕膠帶導致分子掉下來。

趙: 所以只是要看高分子有沒有在上面

ANS:對。

趙: 百格刀怎麼知道高分子有沒有掉?

ANS: 肉眼看起來是整片沒掉，用 IR 看官能基也還在。

趙: P17 (d),(f) SEM 看起來差不多，光 SEM 看的出來有沒有有脫落嗎?

ANS: 因為有做脫落對照組，所以可以比照。

趙: 應該可以用 IR 來看會比較好

64

趙: P16 我覺得要從室溫開始做，像 37~50

ANS: 像 37 度是落在那些範圍裏面。

趙: bio 的話，4~37~50 這幾個溫度比較恰當

ANS:對。

趙:p18 QCM 怎麼做的，他不是要平面的嗎?

ANS: 我們先 coating 在 QCM 晶片上，再跑。